

Chapter 1

Grazing incidence neutron scattering for the study of solid-liquid interfaces

Max Wolff¹, Henrich Frielinghaus², Marité Cárdenas³, Juan Francisco Gonzales³, Katharina Theis-Bröhl⁴, Olaf Softwedel⁵, Regine von Klitzing⁵, Georgia A. Pilkington⁶, Mark W. Rutland⁶, Reiner Dahint⁷, Philipp Gutfreund⁸

¹Department for Physics and Astronomy, Uppsala University, Regementsvägen 1, SE-75120 Uppsala, Sweden

²Jülich Centre for Neutron Science, JCNS-4 at Heinz Maier-Leibnitz Zentrum (MLZ), Forschungszentrum Jülich GmbH, Lichtenbergstrasse, D-85748 Garching, Germany

³Department of Biomedical Science & Biofilms-Research Center for Biointerfaces, Malmö University, SE-20506 Malmö, Sweden

⁴University of Applied Sciences Bremerhaven, An der Karlstadt 8, D-27568 Bremerhaven, Germany

⁵Physik Department, Technical University of Darmstadt, D-64289 Darmstadt, Germany

⁶Surface and Corrosion Science, KTH Royal Institute of Technology, SE-10044 Stockholm, Sweden

⁷Applied Physical Chemistry, Ruprecht-Karls-Universität Heidelberg, Im Neuenheimer Feld 253, D-69120 Heidelberg, Germany

⁸Institut Laue–Langevin, CS 20156, F-38042 Grenoble Cedex 9, France

ABSTRACT

Neutrons are characterised by a low absorption in many engineering materials. At the same time the scattering cross section of light elements, such as hydrogen and deuterium, may be large. These properties make neutron scattering experiments performed under grazing incidence scattering geometry an excellent tool for the study of solid-liquid interfaces. In this review we describe the basic concepts of neutron reflection and grazing incidence scattering experiments as well as experimental procedures and sample cells. The full power of the method is exemplified on a range of science areas, including polymers, bio- and ionic liquid lubricants, electrolytes as well as bio-membranes or magnetic liquids.

KEYWORDS

solid-liquid interface, neutron reflectometry, grazing incidence scattering

List of Acronyms

NR	(specular) neutron reflectivity/reflectometry
SLD	scattering length density
OSS	off-specular scattering
GISANS	grazing incidence small angle neutron scattering
GINSES	grazing incidence neutron spin echo spectroscopy
AFM	atomic force microscope
MG	microgel
IL	ionic liquid
NP	nano-particle
SAM	self assembled monolayer
PS	polystyrene
HA	hyaluronic acid
PE	polyelectrolyte
PDMS	polydimethylsiloxane
LCST	lower critical solution temperature
OTS	octadecyltrichlorosilane
DTS	dodecyltrichlorosilane
PNIPAM	poly(N-isopropylacrylamide)
PDMAEMA	poly(2-(dimethylamino) ethyl methacrylate)
PEM	polyelectrolyte multilayer
PSS	poly(styrene sulfonate)
PDADMAC	poly(diallyl dimethyl ammonium chloride)
PMAA	poly(methacrylic acid)
PMETAC	poly-[2-(Methacryloyloxy) ethyl] trimethylammonium chloride
VPTT	volume phase transition temperature
VPT	volume phase transition
PB	polymer brush
FAIL	fluorinated anion ionic liquid
PTFE	polytetrafluoroethylene
PEEK	polyether ether ketone
PC	propylene carbonate

1.1 NEUTRON SCATTERING IN MATERIALS RESEARCH

Neutron scattering methods offer unique opportunities for the study of structure and dynamics in materials. Unlike x-rays, neutrons interact with the core of atoms via nuclear forces. The neutron has two remarkable characteristics, which are essential for the study of solid-liquid interfaces. First, the absorption in many engineering materials is low, resulting in a large penetration power of neutrons,

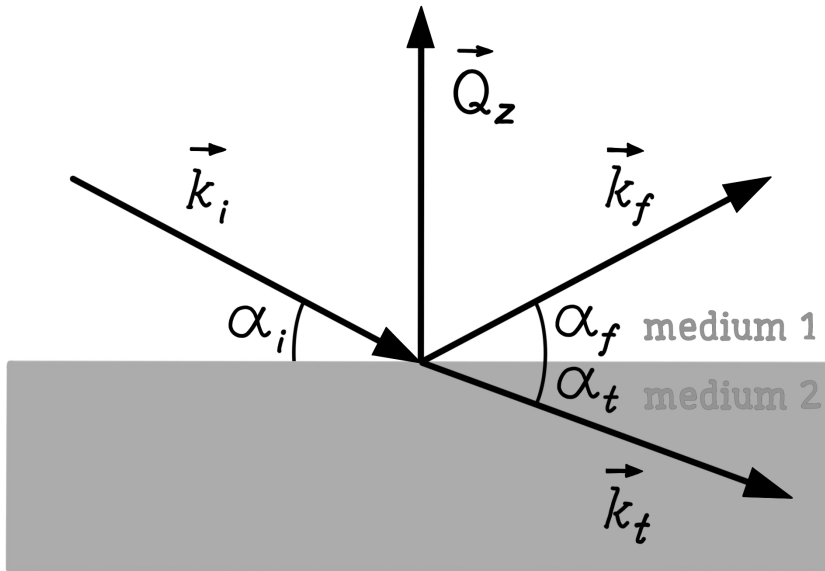


FIGURE 1.1 Scattering geometry for NR measurements.

in particular, for silicon and sapphire. Second, the coherent scattering cross section of deuterium is large, which allows total reflection, for example, from a silicon-D₂O interface.

In this review we explain the principles of neutron reflection (NR) measurements from solid-liquid interfaces and provide experimental details on how measurements are performed. The strength of the method is shown on a range of scientific examples.

1.1.1 Reflection and transmission of neutrons at interfaces

NR measurements concern a neutron beam impinging at a glancing angle, α_i , typically less than 5°, onto an interface. Specular reflection is defined as the intensity reflected from the interface at an exit angle, α_f , equal to α_i . The reflected intensity is plotted versus the momentum transfer, $Q_z = \frac{2\pi}{\lambda} \sin(\phi)$, with λ and ϕ being the wavelength of the neutrons and the scattering angle $\alpha_i + \alpha_f$, respectively. The scattering geometry for NR measurements is sketched in Fig. 1.1. As Q_z is small a continuum approach may be used to calculate the NR by defining a neutron index of refraction. The wave numbers of the reflected and refracted waves are calculated according to:

$$n = \frac{k_t}{k_i} = \frac{\cos \alpha_i}{\cos \alpha_t} \quad (1.1)$$

Material	SLD [10^{-6} \AA^{-2}]
H ₂ O	-0.56
D ₂ O	6.4
Silicon	2.1
Sapphire	5.7

TABLE 1.1 Most relevant SLD values for the study of solid-liquid boundaries.

Here $k_i = 2\pi/\lambda$ symbolises the wave number of the incident neutron beam in medium one and k_t the wave number inside medium two. n denotes the refractive index. The neutron momentum in medium one and two is related to the scattering potential in the respective region. Therefore, n can be calculated from the coherent scattering length b of an isotope and its number density N :

$$n = \sqrt{1 - \frac{\lambda^2}{\pi} Nb} = \sqrt{1 - \frac{\lambda^2}{\pi} \text{SLD}} \quad (1.2)$$

The product Nb is called scattering length density (SLD, see table 1.1 for important values). Note that the SLDs of H₂O and D₂O are significantly different allowing contrast variation experiments, by solvent exchange.

Equation 1.1 allows the definition of a critical angle of total reflection $\cos \alpha_c = n$ as well as a critical momentum transfer $Q_c = \frac{4\pi}{\lambda} \sin \alpha_c = 4\sqrt{\pi \Delta \text{SLD}}$. For a silicon-D₂O interface Q_c is 0.15 nm⁻¹.

For Q_z larger than Q_c the reflection coefficients are calculated as Fresnel coefficients:

$$R_F = \frac{\sin \alpha_i - n \sin \alpha_t}{\sin \alpha_i + n \sin \alpha_t} \quad (1.3)$$

This develops into a Q_z^{-4} decay of the reflected intensity ($I = R_F^2$) for larger Q_z values.

Specular NR, is sensitive to changes in the SLD averaged over the coherence volume of the neutron beam [1]. Assuming Gaussian roughness in the limit of very large in-plane correlation length across an interface, the SLD profile can be described by an error function and the reflection coefficients can be calculated analytically:

$$R(Q_z) = R_F(Q_z) e^{-Q_z^2 \sigma^2} \quad (1.4)$$

The decay in NR is steeper than Q^{-4} .

For layered structures, the reflection and transmission at each interface has to be considered. In 1954, Parratt [2] solved the problem of reflection and transmission at interfaces by developing a recursion algorithm. Nowadays, most fitting programs use the optical transfer matrix method [3, 4].

Fig. 1.2 depicts NRs (left panel) as well as the corresponding SLD profiles (right panel). The black line represents the NR from a bare silicon surface, while the red, dashed line refers to the same interface but with added Gaussian

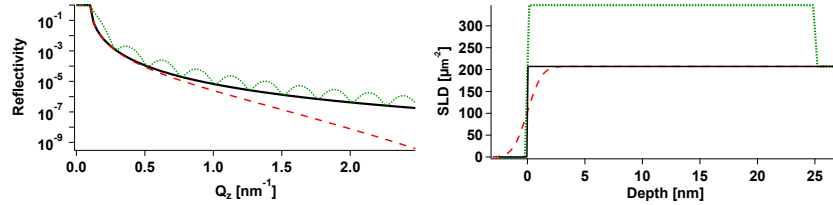


FIGURE 1.2 NR (left) and corresponding SLD profiles for a flat (black, solid line), rough (red, dashed line) and layered interface (green, dotted line).

roughness. The green, dotted line is a simulation done for a flat Si substrate with a flat, 25 nm thick, layer of SiO₂. The difference in Q_z values between consecutive minima of the Kiessig fringes (for larger Q_z values) are a measure of the inverse thickness $d = \frac{2\pi}{\Delta Q_z}$ of the SiO₂ layer.

The spin of the neutron makes it sensitive to the magnetic induction in materials and the refractive index has to be modified by the Zeemann energy:

$$n = \sqrt{1 - \frac{\lambda^2}{\pi} N (b_{\text{nuc}} \pm b_{\text{mag}})} \quad (1.5)$$

The "+" and "-" indicates that the neutron spin is parallel or antiparallel to the magnetic induction. As a consequence, the measured NR depends on the magnetisation in a sample and by analysing the spin asymmetry $\text{SA} = \frac{R^+ - R^-}{R^+ + R^-}$ the magnetic induction in the film can be extracted. The spin of the neutron may also be at an angle with respect to the magnetisation in a film, which will result in a partial depolarisation of the beam allowing measurement of the angle between neutron spin and magnetic induction [5, 6]. Note that, the neutron is not sensitive to the magnetic induction along the direction of momentum transfer. In the absence of a magnetic field, the observed sample magnetization can be attributed to magnetic dipolar interactions between nanoparticles (NPs) in a magnetic fluid. By applying an external magnetic field, the magnetic response of the NPs can be observed.

1.1.2 Off-specular and grazing incidence small angle scattering

Off-specular (OSS) and grazing incidence small angle neutron scattering (GISANS) summarises scattering which is not specular, but still at small Q , and is sensitive to correlations in the plane of interfaces. The scattering geometry is sketched in Fig. 1.3. The specularly reflected intensity is indicated in red. OSS, indicated in green, refers to intensity reflected in the scattering plane at different α_i and α_f . All intensity scattered out of the scattering plane is GISANS, indicated by light blue dots and in yellow.

Fig. 1.4 depicts scattering patterns taken for a micellar solution in a crystalline fcc phase in contact with single crystalline silicon. For more details on the sample

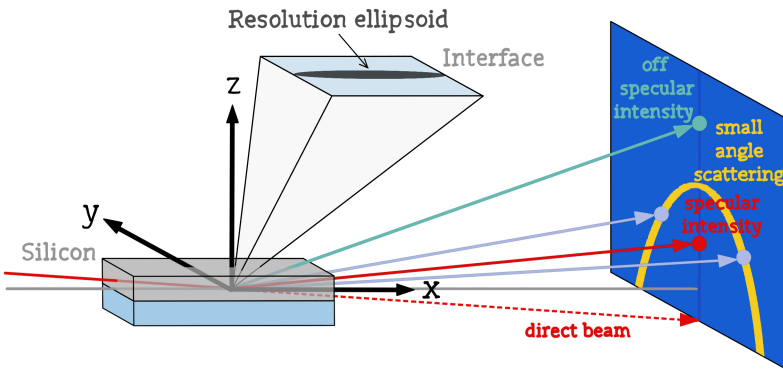


FIGURE 1.3 Scattering geometry for OSS and GISANS experiments from the solid-liquid boundary.

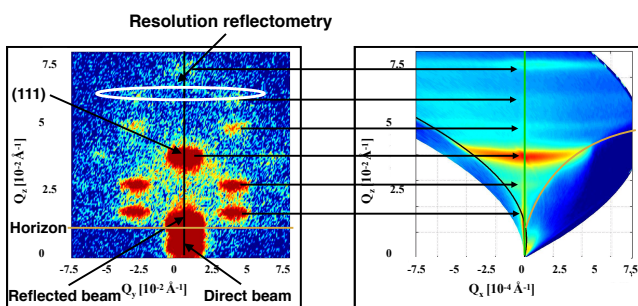


FIGURE 1.4 Scattering patterns for a micellar crystal in contact with a silicon wafer. The panel on the left hand side depicts the GISANS pattern from the cubic close packed structure. The panel on the right hand side depicts the NR and OSS. Fig. reproduced from Ref. [7] with permission from Springer.

we refer to literature [8]. The left panel in Fig. 1.4 depicts a raw detector image taken for one specific α_i and λ . The sample's horizon is indicated by the orange line and the positions of the direct and reflected beams are marked. From the positions of the Bragg spots the cubic dense packing (fcc structure) is revealed. Note, the micellar crystal is not textured (two-dimensional powder) in the plane of the interface. The right panel in Fig. 1.4 shows a NR scan done at constant λ and scanning α_i and α_f . The specular intensity is marked by the green line and the data from the left and right panels intersect along the black lines. The Q ranges, Q_x and Q_y , in the plane of the interface are significantly different. In the right panel the Bragg peaks are smeared out. From the width of the peak along Q_x , the size of the crystallites can be extracted, while GISANS reveals the crystalline structure [9]. Note, the faint intensity visible at positions of GISANS Bragg peaks in the OSS results from the relaxed resolution (white ellipse, Fig. 1.4. left panel) for the NR measurements. The combination of GISANS and OSS allows length scales from about 1 nm to 100 nm and about 10 nm to several tens of μm to be addressed in the direction of the interface, respectively. A more detailed description of OSS and GISANS can be found in Refs. [10] and [11], respectively.

1.1.3 Inelastic scattering

Compared to x-rays, the energy of neutrons with Å wavelength is low. This makes the neutron an excellent probe for the study of low energy excitations, such as phonons, magnons, rotational tunneling or diffusive processes. The spin of the neutron together with a nuclear moment can lead to so called incoherent scattering. This scattering does not provide structural information but rather probes the particle self-correlation function over time and allows the extraction of diffusion constants from the Fourier transform of the line shape of the intensity of scattered neutrons plotted versus energy, so called quasi-elastic scattering. For details on quasi-elastic neutron scattering we refer to literature [12, 13].

Alternatively, neutron spin echo spectroscopy (NSE) probes the coherent scattering signal derived from the Van Hove correlation function of the SLD at two times according to [14]:

$$S_{\text{coh}}(Q, \tau) = \frac{1}{V} \langle \text{SLD}(Q, \tau_0) \text{SLD}'(Q, \tau_0 + \tau) \rangle_{\tau, \text{ensemble}} \quad (1.6)$$

The reference time τ_0 is an arbitrary time that is also a matter of the ensemble averaging (indicated by the angle brackets). Furthermore, we assume the full inversion symmetry of the expression in terms of τ vs. $-\tau$ and Q vs. $-Q$, that usually is fulfilled in all practical cases. The scattering function of the NSE experiment is normalized to the static scattering in order to focus on the bare time dependence:

$$S_{\text{NSE}}(Q, \tau) = \frac{S_{\text{coh}}(Q, \tau)}{S_{\text{coh}}(Q, 0)} \quad (1.7)$$

Then, the measured function starts at unity for $\tau = 0$, and decays monotonically with a typical relaxation time $\tau_{\text{relax}}(Q)$. From the Q -dependence, different underlying motions are distinguished. Examples are simple diffusion ($\tau_{\text{relax}} \propto Q^{-2}$) and membranes in a hydrodynamic medium ($\tau_{\text{relax}} \propto Q^{-3}$) [15].

Compared to structural analysis, neutron spectroscopy typically results in reduced neutron beam intensities and longer counting times. This makes studies of interface dynamics rare and challenging, as the sample volumes are small. Resonant wave field enhancement in a thin film [16] under investigation or at an interface [17] may help to overcome these limitations.

1.2 MEASURING NEUTRON REFLECTION FROM SOLID-LIQUID BOUNDARIES

At large facilities, neutrons are produced either by fission or spallation. Both methods provide high energy neutrons which are moderated to match their energies suitable for the study of interfaces. Fission typically provides a continuous flux of neutrons, while spallation normally results in pulsed beams, which has implications for the instrumentation.

1.2.1 Angle dispersive and time of flight reflectometry

Elastic neutron scattering experiments rely on the measurement of the scattered intensity versus momentum transfer Q , depending on the scattering angle and wavelength. For angle dispersive NR, a monochromatic neutron beam is used and Q is scanned by changing the incident and exit beam angles. To measure the specular NR, the method requires counting each Q_z value separately. Alternatively, a pulsed beam may be used and the wavelength may be determined by evaluating the time of flight (TOF) of the neutrons from the source to the detector. In this mode, a range of Q_z values can be measured simultaneously for one incident beam angle. For most cases, TOF measurements allow faster data acquisition, as the spectrum of the neutron moderator compensates for the steep decrease in NR at larger Q values.

1.2.2 Liquids cells for interface scattering

Compared to synchrotron x-ray facilities, neutron sources provide a much lower brilliance. To optimise the incident neutron flux, relatively large samples are required. For interface studies, the beam impinges onto the sample under a shallow angle resulting in a large interface area intercepting the neutron beam. As an example, a beam of 0.5 mm width impinging onto a sample at an angle of 1° results in a beam footprint on the interface of about 3 cm.

To enable the investigation of solid-liquid interfaces dedicated equipment is required, which allows the transmission of a neutron beam through a solid substrate and reflection from a liquid boundary. The neutrons are typically

transmitted through a silicon or sapphire crystal of rectangular shape and a thickness of about 1 cm, to ensure the same path length for all neutrons. The surface area of the crystals is typically 25 - 100 cm², which requires sophisticated polishing procedures to achieve the required surface roughness of less than 1 nm. Some more details on a specific solid-liquid cell for NR studies can be found in Ref. [18].

As a large dynamic range needs to be measured in NR, a particular challenge is background, which may arise from the crystal as well as from the liquid sample. Typically, liquids contain significant amounts of hydrogen, which scatters strongly incoherently, leading to an enhanced background for the reflectometry measurement. To overcome this challenge, a low background liquid cell with reduced liquid thickness that minimises incoherent scattering from the liquid sample has been developed [19].

1.2.2.1 Electric fields

The application of electric fields requires that the active interface under investigation should in principle act as an electrode. While silicon has semiconductive properties it is experimentally easier to provide a reproducible applied potential using the gold films commonly used in NR; a consequence of this is that the cell design should allow a small portion of the gold coated silicon block to be exposed outside the liquid enclosure. This has led to the use of O-ring or gasket designs, not unlike those in conventional liquid cells. The cell design used for the electroresponsive interfacial self assembly of ionic liquids (IL) is depicted in Fig. 1.5 [20].

To provide a uniform electric field across the cell, and perpendicular to the interface, the gasket should seal against a counterelectrode opposite the working electrode (gold surface). A convenient material for this purpose is conductive glass since it is relatively inert, but also provides the opportunity for visual inspection of the cell, for example to detect bubbles or deterioration of the gold surface. It also assists when filling the cell since the wetting of the liquid can be followed, and for liquids with differences in refractive index it is possible to observe "plug flow" replacement of the liquid contents. It is recommended that a C-V Current-Voltage experiment is performed either before or after (or both) to ensure that the system is inside the electrochemical window expected. To avoid embarrassing incidents such as the "in operando study of the electroplating of glass with gold" it is advisable to monitor the current using the potentiostat employed to apply the variable electrical potential.

1.2.2.2 Confinement

The study of soft matter films under mechanical confinement was originally made possible by the development of the Surface Force Apparatus [21] and the Atomic Force Microscope (AFM)[22, 23]. While these techniques procure accurate interaction forces at different separations, their ability to provide structural

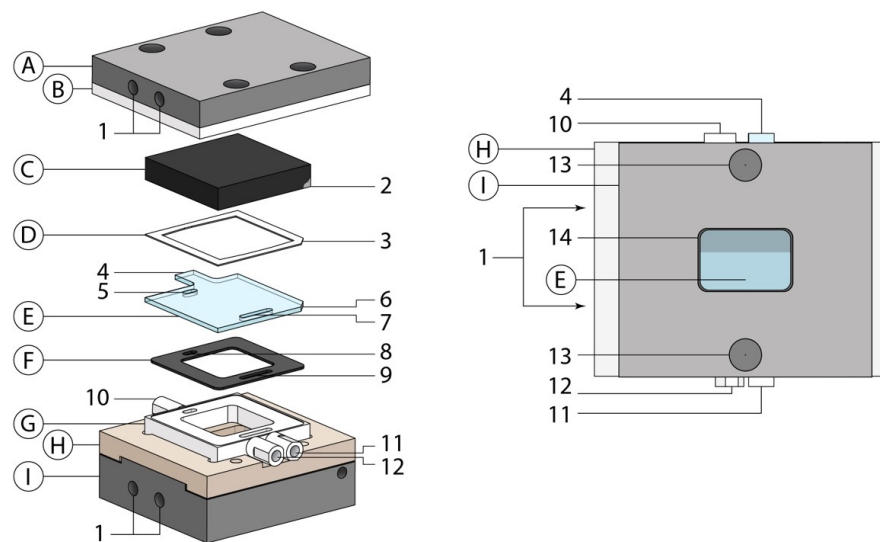


FIGURE 1.5 Electroresponsive NR cell. Reproduced from ref. [20] with permission from the Royal Society of Chemistry.

Parts: A, I: aluminium outer shell. B: PTFE seat for C: gold coated Si block. D: PTFE gasket. E: counterelectrode (glass). F: Kalrez gasket. G: PTFE spacer unit. H: PEEK recessed plate. Features: 1: water cooling. 2: exposed corner of block for wire attachment. 3: truncation of gasket (wire accommodation). 4: extension of counterelectrode for wire attachment. 5-9: Liquid channels for filling/liquid exchange. 10-12: syringe ports. 13: locator bolts for beam mounting. 14: Window

information is limited. Further insights beyond the measurement of forces and resolving near-interface structures has been a challenge until recent developments. One of the main difficulties of combining surface force measurements with other information has been to achieve a reproducible confinement within the limits of the employed technique (geometry, sensing probe, etc.). A breakthrough in this direction was the development by Cosgrove and collaborators [24, 25, 26] of a confinement device operated in NR. This setup required two quartz plates between which the sample was placed, while the pressure was controlled by a hydraulic ram. A number of variations of the confinement cell has been proposed since then [27, 28]. However, these setups were bounded by several aspects that limited an improvement of the distance between the plates: the long range waviness of the plates, the proneness to misalignment of the opposing surfaces and the presence of dust. A new improvement was recently achieved thanks to a design by de Vos et al. [29], where the applied pressure can be set between 1 to 10 bar. In the new setup (see Fig. 1.6), one of the rigid plates was replaced by a flexible membrane (Melinex® 401, DuPont, Teijin Films), characterized by a flat surface, excellent mechanical properties and high chemical homogeneity ($SLD = 2.53 \cdot 10^{-6} \text{ \AA}^{-2}$). Under pressure, the membrane is able to adapt to the long-range waviness of the opposite surface and bend around any deposited dust, thus improving control of the separation between the surfaces and the confinement of the sample. The improved version of the confinement cell has been successfully used for a number of investigations trying to elucidate the structure of soft matter systems under confinement: poly-electrolyte multilayers [30, 31], polymer brushes (PBs) [32, 33, 34] and mucins films [35]. Also, the modified device has been tested for GISANS experiments and different geometries at the Institute Laue Langevin (Grenoble, France) in preparation for a new development of the confinement cell that will implement shear. Despite the achievements, the limitations of the device have been shown in recent experiments [35] where low confinement pressures are required. In the same way as the AFM requires different types of cantilevers to explore a variety of samples, the new confinement cell will need a number of membranes with different mechanical properties to explore confinement at different pressure ranges.

1.2.2.3 Rheology

To enable investigations of the solid-liquid interface when a deformation or shear is applied to a liquid, rheometers have been adapted to the needs of NR measurements [36]. As large areas are probed, a cone-plate geometry is preferable to ensure a constant shear rate across the interface. For volatile liquids or solvents, a solvent trap may be used.

A sketch of a rheology adapter is shown in Fig. 1.7. The key modification to the rheometer is at the base plate (non rotating surface). To allow the neutron beam to impinge on the liquid interface, a thick and large silicon substrate is clamped to an aluminum holder. This holder is designed to fit the standard

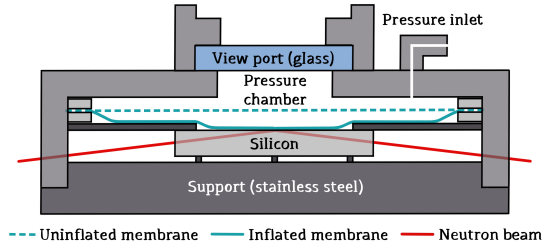


FIGURE 1.6 Sketch of the confinement cell developed for NR experiments.

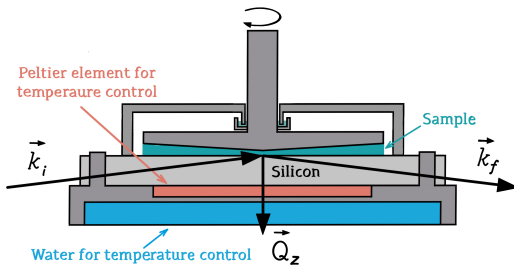


FIGURE 1.7 Sketch of the geometry for combined NR and rheology experiments.

fixation of the base plate of the rheometer and attached to the water or nitrogen cooled base. For additional temperature regulation, a Peltier element is located directly under the silicon crystal. An advantage of this design is that the solid substrate can be changed easily in order to allow different materials and surface terminations. In combined rheology and reflectometry measurements, Q_z is parallel to the shear gradient. Off-specular and GISANS probe in-plane structures along or perpendicular to the flow by using a center or off-center beam geometry, respectively.

Most rheometers can apply both continuous or oscillatory shear to probe viscoelastic properties. In the oscillatory mode, a periodic stress is applied to a sample and cyclic neutron experiments can be performed by registering the time the neutron scatters from the sample together with the stress state. This approach allows a histogram of the neutron events with respect to the stress applied to the sample, with time resolution down to ms [37].

1.3 THE SOLID-LIQUID BOUNDARY INVESTIGATED BY NEUTRON SCATTERING

NR can be applied to a wide range of solid-liquid boundaries. In this chapter we review some recent results.

1.3.1 Hydrodynamics and lubrication

1.3.1.1 Depletion

With improving experimental sensitivity a debate on the nature of the solid-liquid boundary emerged and, in particular, whether a liquid in contact with certain solids may locally change its density. Such boundary effects are of high relevance for interfacial water, which plays a key role in biological processes [38] as well as for the design of microfluidic devices [39]. The study of different model hydrophobic surfaces in contact with water has lead to controversial results on whether a density depleted layer of water exists [40]. To quantify potential depletion effects, the so called depletion distance was defined:

$$d_{\text{depl}} = \int \left(1 - \frac{\rho(z)}{\rho_{\text{bulk}}}\right) dz \quad (1.8)$$

with ρ the density of the liquid. NR provides a direct measure of densities and the depletion distance. From a NR study on a spin coated polystyrene (PS)-D₂O interface, a depletion distance of 2.6 Å was extracted [41]. However, a reproduction experiment with a freshly prepared PS surface (never exposed to air) by a different group did not confirm the presence of a depleted layer [42]. It may be concluded that a depleted layer, if present at all, might occur on a submolecular level.

The situation becomes even more complicated if the water is supersaturated with gas, which may condense at the hydrophobic substrate [43]. Indeed such condensation was detected experimentally in the form of nano-bubbles [44] which were imaged by AFM [45, 46]. However, it was debated that the nano-bubbles were actually created by the AFM tip, which needs almost direct contact with the surface under investigation but X-ray reflectivity measurements provided controversial results [47, 48] as well. Over time, nano-bubbles were detected with less invasive techniques like infrared [49] and optical [50] spectroscopy. It is currently accepted that nano-bubbles may be produced locally at a solid-liquid interface [51] but their time and space average and relevance for microfluidics and cell biology is still debated [52]. Due to the large SLD of D₂O and the reported size of 50-10000 nm of the nanobubbles they may be well studied with NR, GISANS and OSS but no evidence of time or space averaged nano-bubbles was found following existing protocols for nano-bubble creation [53].

1.3.1.2 Hydrodynamic boundary condition

A density difference in a liquid close to a solid substrate affects the local viscosity and the flow profile close to an interface. Similar to a depletion distance one may define the slip length as the distance in front or beyond a solid interface at which the velocity profile of the liquid extrapolates to zero. If one assumes a depleted layer as the only reason for the interface anomaly the slip length can be directly related to the depletion distance d_{depl} [54] and is accessible to NR.

NR experiments were performed on hexadecane in contact to a silicon interface with different coatings tuning the surface energy [55, 56]. No changes in the density of the liquid were found close to the interface for shear rates up to 500 s^{-1} . In contrast to previous surface force apparatus measurements [57], much smaller values for the slip length were found. In addition, a decreasing slip length was reported for increasing surface energies, which contradicts the earlier findings. Thus it seems that density depletion may not explain interface anomalies in the hydrodynamic boundary condition.

Surface anomalies in the hydrodynamic boundary condition might be related to the conformity of lateral correlations with characteristic distances of the liquid molecules. Interestingly, a significant difference in slip length was reported for PS sliding past octadecyl-(OTS) or dodecyl-trichlorosilane (DTS) self assembled monolayers (SAM) during dewetting. This is a surprising result as OTS and DTS are almost identical molecules only differing in the length of the carbon backbone. However, it was shown that OTS may grow with a pseudorotational epitaxy and form an extremely well ordered SAM [58]. From a combined x-ray and NR study, it turned out that a well ordered SAM allows the phenyl rings of PS to enter and anchor leading to the reduced surface slip [59].

1.3.1.3 Boundary lubricant properties of ionic liquids

ILs have been proposed as potential next generation lubricants [60] since they fulfil many criteria: They form load supporting self-assembly films at interfaces and are (generally) chemically robust with low vapour pressure and high thermal stability [61]. An additional attractive characteristic is that they provide the potential for control of friction using electric fields, due to their inherently ionic nature - so called "tribotronics" [62]. The area of electroactive friction has been recently reviewed by Spikes [63]. The use of ILs in this context is rather recent, and has been well demonstrated at the nanotribology level using AFM in both pure ILs and with additives [64]. Briefly, an interface interrupts the bulk structure of ILs, and the interfacial structuring can be thought of as akin to adsorption. When ILs are dissolved for example in a polar oil, then the interfacial structure is equivalent to adsorption. When this interface is also an electrode then the application of electrical potentials to the surface results in the exchange of ions between the interfacial layer and the bulk *e.g.* the composition of the interfacial layer is controlled by the electrical bias, and in turn the frictional properties of a contact can be controlled [64]. Since the ions are relatively large compared to the area of surface charge sites, the ordering of the IL layers in response to the surface charge can extend several ionic layers away from the interface [65].

NR with its ability to resolve structure/composition perpendicular to the interface thus provides a unique opportunity to study the interfacial, and near interfacial ordering of ILs, particularly as additives for example to a polar solvent or model oil where there is contrast between the oil and the IL. In the pure IL, the contrast is generally poor since the interfacial species also comprise the

bulk liquid - however if the anion and cation have significantly different SLDs then they can be distinguished [66]. As an additive to a model oil the IL trihexyl(tetradecyl)phosphonium bis(2,4,4-trimethylpentyl)phosphinate in octane was used and NR [67] with multiple contrasts to study the interface on an oxidized silicon block. It was possible to observe a thin adsorbed layer with a temperature dependent thickness of the order of 10 Å and containing around 22 mol% solvent. In contrast, gold surfaces have been used to study the electroresponsiveness of the adsorbed IL layer. From a tribological perspective, fluorinated anion ILs (FAILs) need to be avoided and here we address anions based around orthoborate anions [68], with either phosphonium or imidazolium cations. The solution conditions are matched to gold by considering the SLDs of the dissolved ions and their concentration and then mixing deuterated and undeuterated solvent.

The interfacial film consisting predominantly of IL provides a contrast layer and a reflectance profile consisting of Kiessig fringes. The application of a potential within the electrochemical window changes the composition and thickness of the IL interfacial layer, which in turn modifies the contrast of the layer since the anions and cations have rather different SLDs. As an example, the IL PBMB has an SLD of $0.5 \times 10^{-6} \text{ \AA}^{-2}$ whereas the cation has an SLD of $-0.4 \times 10^{-6} \text{ \AA}^{-2}$ and the anion an SLD of $2.68 \times 10^{-6} \text{ \AA}^{-2}$ [69]. Changes in the SLD can thus be clearly related to changes in the relative numbers of anions and cations in the layer (see Fig. 1.8). Acetone as a polar solvent did not produce dramatic electroresponsivity but proved the principles and established the methodology [20]. Propylene carbonate proved a better solvent and the deuterated version is available commercially. It was first used to demonstrate the concentration dependence both of the layer properties and their electroresponsiveness [69]. The electroresponsiveness was much greater than in acetone and at higher concentrations (20% w/w) there were many more ions in the interfacial film than at lower concentrations. As the field was applied, the SLD of the layer changed dramatically (at negative potentials a thin layer dominated by the cation SLD) and at positive potentials a much thicker but more diffuse layer was observed with an SLD more influenced by the anion. AFM was used in the same study to demonstrate that the frictional properties change systematically with the ion composition inferred from the NR. When the cation, which has inherent self-assembly properties, was at the interface, the friction was lower, and as its relative abundance in the interfacial film reduced, the friction of the layer increased. This knowledge can be used to design responsive friction systems.

The combination of NR with vibrational sum frequency spectroscopy has rarely been attempted, since both are extremely demanding techniques, but when this is done the combined chemical and orientational message is very powerful [70, 69]. It was shown that the chain length of an imidazolium IL strongly affected the structure of the interface layer, with C10 chains forming centro-symmetrical bilayer structures at the interface which shorter chains were incapable of. Furthermore, it was possible to observe the changes in the orien-

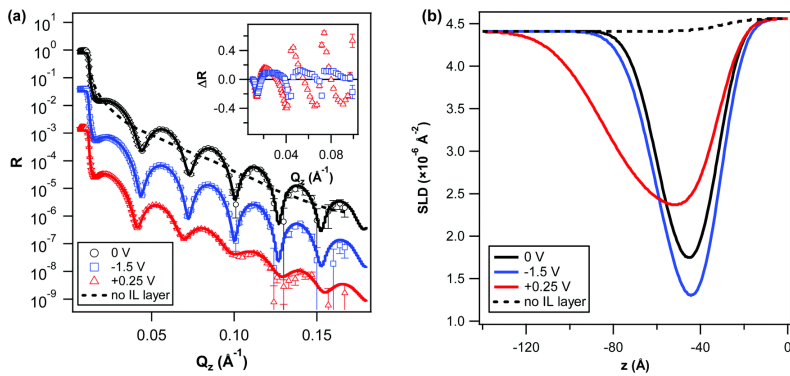


FIGURE 1.8 Panel a: Effect of applied potential on NR for 20% w/w [P6,6,6,14][BMB] in PC ("gold matched bulk". Note that 20% is a sufficiently high concentration that a perfect match cannot be achieved even using pure deuterated PC). The symbols are experimental data, lines are best-fits to the data. The curves are offset to facilitate comparison and the error bars reflect the standard deviation. The dashed line indicates the expected reflectivity in the absence of an interfacial IL layer. Inset: Asymmetry plots $\Delta R = [R_V(Q_z) - R_0(Q_z)]/[R_V(Q_z) + R_0(Q_z)]$, indicating the change in reflectivity upon applying a potential, compared to the data at 0 V. Panel b: SLD profiles obtained from the fits to a single layer model. $z=0$ corresponds to the gold-solution interface. At negative potentials the SLD of the layer decreases since the cation has a lower SLD, indicating a consolidation of cations in the layer. At positive potentials there is a clear change in the structure with broadening as well as a reduction in SLD, indicating a change in the interfacial structure as well as a higher anion content. Reproduced from ref. [69] with permission from the Royal Society of Chemistry.

tation of the (positively charged) imidazolium ring at the interface as the surface potential was adjusted.

Finally, as a molten salt, contamination by water is a significant problem, and this is predicted to affect the nanotribological response of the interface, depending on the location of the water molecules, which of course adapts to the (voltage dependent) IL ordering [71]. Because of this, all the electroresponsive experiments were prepared in a glove box with RH < 10% and the samples dried in a vacuum oven prior to use. However, to mimic the effect of water, D₂O can be added to the solutions to see how this affects both the water content and the interfacial ordering/layering. As the only species with an SLD greater than that of the gold and the gold matched bulk, its presence and location could clearly be identified in the SLD profile. Interestingly, the presence of water appears to favour the formation of discrete layering and assist the so called crowding structure predicted for pure (dry) ILs [65]. This information explains the tribological observations - water reduces the lubricating ability (the friction coefficient increases), but the electoresponsivity becomes much more pronounced with much lower friction for the well defined cationic layers at negative potentials.

1.3.1.4 Biolubricants

Efficient mechanisms of lubrication in the human body are essential to maintain health for decades of lifetime. A prominent example is joint movement, where increased friction and wear can lead to osteoarthritis, the most common musculoskeletal disease in many developed countries [72]. With friction coefficients of about 0.001 to 0.01 for operational conditions ranging from resting state to rapid motion and low to high applied load, lubrication in natural joints far outperforms typical artificial systems [73, 74, 75]. It is, therefore, of high interest to elucidate the mechanisms of joint lubrication on a molecular scale, also in view of bio-inspired improved technical solutions.

In mammalian joints, the gap in between the opposing bone ends is filled with the synovial fluid, mainly composed of hyaluronic acid (HA), aggrecan, lubricin, and phospholipids [74, 76]. The bone ends themselves are coated with cartilage, which in turn is covered with a layer of phospholipids, glycosaminoglycans (such as HA) and proteins [77]. It is widely assumed that this layer, interacting with the synovial fluid, is the main source of highly effective lubrication.

NR measurements on confined lipid bilayer stacks indicate that, even at pressures up to 5 bar, the bilayers are separated by a thin water layer. This supports the relevance of lipid hydration in joint lubrication [78]. The thickness of the lipid layer increases with pressure and the lipids seem to adopt a more closely packed state. Combined NR, infrared spectroscopy and ellipsometry studies show that both HA and polyelectrolytes (PE) - serving as polymeric analogues for HA - adsorb onto the headgroups of oligolamellar lipid bilayers and induce significant swelling of the film [79, 80]. The interlamellar distance of

the bilayers is well described by the interplay of associated Coulomb repulsion and attractive van der Waals forces [80]. Compared to measurements in pure D₂O, HA and PE exposure stabilizes the lipid films with respect to temperature increase and mechanical stress [79, 81, 82]. It is suspected that PE and HA penetrate and interconnect the lipid layers so that a hydrogel is formed which protects the cartilage and prevents osteoarthritis. Also, a phase transition of the lipid layers from their gel state P_{B'} to their fluid state L_α has been observed for increasing shear [81].

Lubricin is a linear molecule consisting of a heavily glycosylated mucin-like core flanked by a 2-somatomedin B (SMB) domain at the N terminus and a haemopexin (PEX) domain at the C terminus. NR studies indicate that it binds to silicon substrates via its end domains yielding a mucin-like loop structure at larger distance from the interface [83]. If calcium ion content is increased from zero to concentrations higher than those in the synovial fluid of healthy joints, the water content of the mucin regime is strongly reduced. Concomitantly, the interfacial layer thickness significantly increases and the films roughen as observed in AFM measurements. Combined NR and atomic force spectroscopy measurements on mechanically confined mucin films prove their almost complete compression and dehydration at 1 bar [84]. The importance of calcium ion content has also been demonstrated for surface-grafted HA, where increased ion concentrations induced a strong collapse of the HA chains, resulting in an enhanced polymer density close to the interface [85].

As shown by selected examples, NR can provide detailed insight in the structure and composition of lubricating films in biorelevant systems. However, the relative importance of the various compounds, potential synergistic effects, and the detailed mechanisms of wear reduction are still a major field of research [86]. In future NR studies, deuteration of selected molecules can help to discriminate the contribution of individual species to synergistic behavior.

1.3.2 Polymer interfaces

1.3.2.1 Polymer Brushes

Polymer decorated surfaces are getting increasingly important in many current technologies [87]. Due to its atomic resolution, non-invasive nature and the possibility to enhance the contrast between different components of interfacial films or solvent and layer by isotopic replacement, NR is a powerful tool for the structural investigation of complex interfaces. Therefore, the monomer density profiles of end-tethered chains in solution were mainly revealed by NR on PS brushes, first on physisorbed diblock copolymers [88, 89] and later on (PS) brushes chemically grown from the surface by atomic transfer radical polymerization [90, 91, 92]. PS was also used to unravel the monomer density profile in star polymers [93] and even the chain-end distribution by appropriate monomer labelling [94], both in deuterated toluene as solvent.

Another polymer used is polydimethylsiloxane (PDMS), either irreversibly adsorbed (pseudo brush) [95] or one-end-tethered [96] onto solid substrates. More recently, polymers undergoing a lower critical solution temperature (LCST) like poly(N-isopropylacrylamide) (PNIPAM) were studied as candidates for stimuli-responsive brushes, and their monomer density profiles were extracted by NR [97, 98, 99, 100, 101] as a function of temperature in water.

Another advantage of neutrons is that many engineering materials are transparent to neutrons allowing for complex sample environment making *in situ* or *in operando* measurements possible. This enables e.g. structural investigations of polymer brushes (PBs) under shear load. These have been mainly performed by NR measurements on PS brushes. Initially, these studies focused on *in situ* shear in pure solvents [102, 103, 104, 105, 106, 107], where no change of the grafted layer was observed. Later, *in situ* sheared PS brushes in contact with a semi-dilute PS solution [108] showed a reproducible retraction of the brush from the bulk liquid under shear in line with a loss of entanglement.

Another sample environment frequently used in NR investigations of PBs are pressure cells. The studies using these include brushes solved in supercritical carbon dioxide under pressure [109], and the temperature and pressure dependence of a poly 2-(dimethylamino) ethyl methacrylate (PDMAEMA) brush which also exhibits a LCST when exposed to water [110].

Brush structures under confinement became recently accessible by NR in the case of two brushes in close contact using a polymer membrane (see section 1.2.2.2) [32, 33] or a floating brush [111, 112].

1.3.2.2 Polyelectrolyte Multilayers

Polyelectrolyte multilayers (PEMs [113]) are thin films made of successive adsorption of oppositely charged polyelectrolytes by dipping, spraying or spin-coating from aqueous solutions.

NR is well suited for investigations of the structure of PEMs at air-solid [114] and solid-liquid interfaces [115, 116]. Especially the isotopic labeling of at least one of the polyions reveals that neighbouring, oppositely charged, layers in PEMs are blended, and that the interdigitation of adjacent bilayers can be tuned during preparation from complete intermixing to well determined layer-wise structure [117].

NR is also used to shed light on the build-up process. For instance mixing short protonated poly(styrene sulfonate) (PSS) and long deuterated PSS in the polyanion adsorption solution and using poly(diallyl dimethyl ammonium chloride) (PDADMAC) as polycation results in PEMs with an adsorption time dependent SLD. Short polyanions adsorb faster and are exchanged against their longer counterparts during the adsorption process. This result is in agreement with the higher mobility of the short chains and lower loss in entropy for longer chains after adsorption [118]. Also a homogeneous counterion distribution across the PEM was found [119]. Quantifying the solvent volume ratio from

the refined SLD and swelling behaviour of the PEMs gives information about residual water and voids as well as about possible deuterium/proton exchange [120, 121]. Moreover, the swelling ability depends on a variety of preparation conditions ranging from polycations and polyanions used, their molecular weight, type and strength of salt added, pH and temperature, hydrophobicity of the outermost layer and thermal post treatment of the PEMs [116, 122].

The combination of isotopic labeling and high spatial resolution allows NR to quantify slow diffusion processes across PEM along the interface normal, studying either superposition of several repeating units or a single interface between deuterated and non-deuterated layer stacks [123, 124]. Both approaches show that refining the SLD, using analytic functions that solve Ficks 2nd law, links the time evolution of the interfacial width between deuterated and non-deuterated layers, with the diffusion constant along the surface normal. Subsequent studies investigated the impact of polyion chain length, incorporated branched polyions as diffusion barriers, initial conformation of the polyion layers and the impact of high ionic strength on the vertical diffusion constant. Thereby the diffusion coefficient in PEMs can be altered over a wide range ($D \approx 10^{-22} \dots 10^{-18} \text{ m}^2 \text{s}^{-1}$) in PDADMAC/PSS-PEMs [125, 126, 127]. Similar diffusion coefficients were found in PEMs made from PDMAEMA and poly(methacrylic acid) (PMAA). A systematic investigation of these PEMs revealed that the diffusion constant scales exponentially with the (monovalent) salt concentration of the annealing solution ($D \sim e^{[NaCl]}$) [128].

Due to reversible swelling and deswelling of most PEMs, for the sake of better contrast, lower background and less sample environment requirement, most of these studies are carried out at the (dry) air-solid interface, but in principle they can also be carried out at the solid-liquid interface.

1.3.2.3 Polymer brush - composites

Combining PBs and PEMs to coat interfaces has the potential to keep the advantages of the PBs mechanical stability of covalent grafted brushes while maintaining the flexibility to functionalize them with PEMs or nano-carriers to design multiresponsive coatings. Consequently mutual interactions between the compartments and compounds have to be considered. Thus, adsorption of PDADMAC/PSS-PEMs onto the temperature-dependent PNIPAM-PBs shifts and broadens the volume phase transition (VPT), although it does not completely extinguish the thermal response, as revealed by NR [129]. NR serves also to determine the amount and distribution of residual water in these composites and the uptake can be selectively tailored [130]. The technique is also successfully applied to investigate the spatial distribution of incorporated gold nano-particles (AuNP) in PNIPAM-PBs and gives valuable input to explain (non-)reversible optical response, while cycling around the VPT temperature (VPTT) [101]. It was shown that the actual distribution of negatively charged AuNP, embedded

in the cationic poly-[2-(Methacryloyloxy) ethyl] trimethylammonium chloride (PMETAC) brushes, can be varied by changing the electrostatic interaction via e.g. pH or salt during adsorption [131].

1.3.2.4 Microgels

Microgels (MGs) addressed here are hydrogel particles with a diameter of several tens of nanometers up to a few micrometers built up of NIPAM or oligo(ethylene glycol methacrylate) (OEGMA) units. The amount of cross-linker controls the stiffness of MGs. The charge and hydrophobicity can be adjusted by additional co-monomers. They show a LCST-like VPT and depending on their composition, the VPT temperature (VPTT) can be adjusted between 20 and 90 °C. They are spin-coated on a planar (silicon) substrates which allows control of the MG number density by the rotation speed. The structure of densely packed layers, *i.e.* the thickness, density and roughness is studied by NR against D₂O [132]. GISANS allows detailed studies of the internal structure of the MGs. The scattering curves can be described by the superposition of two functions with two different characteristic lengths: The Ornstein-Zernicke function contains the correlation length ξ (5 - 10 nm) referring to the thermal fluctuation of the polymer network and the Debye Bueche function addressing the size Ξ of frozen inhomogeneities (10 - 100 nm). While MGs with a rather homogeneous structure show similar values for ξ and Ξ , the difference between the two lengths increases with increasing heterogeneity. Adsorption of the MGs stretches the network leading to an increase in ξ . This flattening is more pronounced for MGs with lower cross-linker density, *i.e.* for softer gels [133]. Due to stronger flattening and stretching softer MGs show reduced dynamics of the polymer network in comparison to stiffer MGs [134]. The dynamics are measured by grazing incidence neutron spin echo spectroscopy (GINSES) and allows scanning the dynamics profile perpendicular to the substrate interface by varying the angle of incidence [134, 135]. A reduction of dynamics is detected close of the substrate interface and increases towards the value for MGs in the bulk phase by increasing the angle of incidence and crossing the angle of total reflection. In contrast to MGs in bulk solutions, the reduced dynamics at interfaces suppress the critical slowing down, *i.e.* divergence of ξ , close to the VPTT [136].

1.3.3 Colloidal particles

1.3.3.1 Magnetic nano-particles

Colloidal suspensions of magnetic particles with a size of a few nanometers are called ferrofluids. The particles are typically smaller than the minimum size of a magnetic domain and are therefore likely to be in a single domain magnetic state [137, 138]. Due to thermal motion, the magnetic moments of the particles are randomly aligned in the absence of an external magnetic field, and the fluid as

a whole exhibits paramagnetic behavior. Usually, the nano-particles (NPs) are suspended in a carrier fluid such as oil, water, or others and coated with ligands. This geometry leads to competition between magnetic and steric interactions, resulting in strong correlations between magnetic and translational degrees of freedom. By applying an external magnetic field, the individual NPs align their magnetic moments along the field lines [139], while the dipolar interaction simultaneously leads to an ordering of their positions in space.

Well-ordered NP ensembles in ferrofluids can be generated by self-assembly. Self assembly is a method that provides controllable, simple mechanisms for the arrangement of magnetic NPs into ordered structures, which can be achieved either through the direct interaction of the building blocks or by using a template or external magnetic fields [140, 141, 142, 143].

To study the self-assembly of magnetic NP structures on solid surfaces under the influence of a magnetic field, (polarized) NR is a unique tool to characterize depth-dependent profiles of the averaged nuclear structure and the magnetization. Quantitative analysis of (polarized) NR data in conjunction with model calculations of the arrangement of NPs in the layers allows characterization of the dimensions of the core/shell NPs and the arrangement of NPs in the layers as well as the magnetization depth profile.

Several studies show that a robust, densely packed wetting layer [144] can be generated by a variety of surface interactions, both chemical [145] and magnetic [146], and that its properties can be controlled by various parameters such as particle size and symmetry [147]. The structure of the subsequent layers varies to a greater extent depending on the solution properties and the characteristics of the surface interaction [148, 149].

The magnetic field-dependent magnetization of the individual NP layers depends on two factors, one being the rotational freedom of the layer and the other being the magnetization of the neighboring layers. For layers where the NPs can rotate more freely, the easy axis of the NP can easily orient along the field direction. With denser packing, the free rotation of NPs is hindered, and the NP ensembles likely form quasi-domain states to minimize energy, resulting in lower magnetization in these layers [148, 149].

1.3.4 Self assembly and model membranes

Surfactants are amphiphilic molecules, which have a strong tendency to self assemble for higher concentrations in a solvent. This self assembly can be well studied with neutron scattering methods and, in particular, small angle neutron scattering is used to identify the different phases. At a solid interface the structure and the dynamics of surfactants may change, depending on the properties, surface energy, roughness or charge state.

1.3.4.1 Model membranes

NR gives the density profiles of supported, tethered or floating supported lipid bilayers (SLBs). The first case is popular because supported SLBs can easily be constructed from simple and reproducible methods such as vesicle fusion. Tethered and floating SLBs often require more complicated deposition methods such as Langmuir-Blodgett [150] but also improve the mimicry aspects of these model cell membranes. The lipid head groups and acyl tail region of the lipid bilayers can be clearly resolved since there is enough contrast due to the distinct atomic composition between the tail and head and these are aligned in layers parallel to the solid-liquid interface. There is even enough contrast to distinguish, for example, protein penetration in the tail region. The contrast, however, can be enhanced by the use of deuterated lipids. Besides providing detailed information on the structure of SLBs themselves as a function of composition [151, 152, 153], SLBs can be used to characterise the mechanism of interaction with biomolecules such as peptides and proteins as well as NPs [154]. Since NR is sensitive to the composition of the lipids in the SLBs, this technique is very powerful to follow exchange processes and has been applied to map lipid flip-flop and exchange processes with lipid based nano-assemblies by using both hydrogenated and deuterated lipids [155, 156, 157]: this is not only the total exchange but particularly how many lipids are removed versus deposited as the amount of solvent can be deconvoluted when collecting multiple solvent contrast data. For example, very recently NR was used to demonstrate that the spike protein in SARS-CoV2 interacts with high lipoprotein density (HDL) particles and that affects the HDL's lipid exchange capacity towards model membranes[158].

In 2002, Pabst et al. [159] applied GISANS to follow the lamellar repeating distance for a multilayer stack of phospholipids at a solid surface as a function of temperature and compared to the repeating distance obtained by small angle scattering data from multilamellar vesicles. The authors observed a smooth swelling from 64 Å at room temperature to about 68-69 °C, after which the diffraction signal was lost due to unbinding from the vesicles, probably due to the formation of vesicles in solution.

Later, in 2015, similar methodology was used by Jaksch et al. [160] to study the effect of ibuprofen addition to phospholipid multilayers on a solid surface. The data showed that as the ibuprofen concentration increased up to 25 mol%, the disorder in the lamellar phase increases, which is evident through the appearance of Debye-Scherrer rings probably due to tilted lamellar formation. Above 34.5 mol%, a hexagonal structure starts to appear coexisting with the lamellar phase until only a hexagonal lattice is retained above 50 mol%. NR and GISANS has lately been combined with GINSES to characterise both the structure and dynamics of multilayer stacks [161, 162, 163]. For example, it was found that increasing the NaCl concentration changes not only the water-headgroup interface and the interlamellar distance but also the inter-plane viscosity. Using

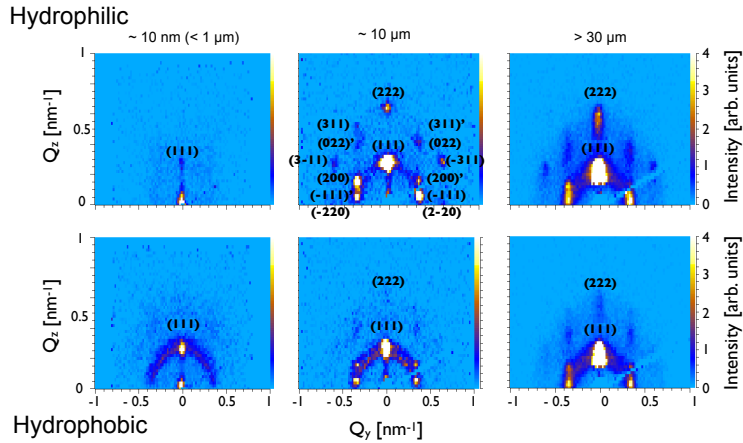


FIGURE 1.9 GISANS patterns for a crystalline micellar structure in contact with silicon surfaces with different surface energy. Texture is more pronounced at the hydrophilic surface (see center panels) and decays with increasing distance from the substrate (left to right). Fig. reproduced from Ref. [164] with permission from the International Union of Crystallography.

this new knowledge, the dynamic behaviour of membranes can be understood and modelled in terms of inter-plane viscosity, which strongly supports the existence of a thermally excited mode in phospholipid membranes for close to physiological conditions. Caselli et al. [154] combined NR, GISANS and fluorescence microscopy to characterise the interaction of NPs with membranes of different topology. 2D symmetric or 3D symmetric membrane topology was modelled by the use of either (planar) multilayers of phospholipid-based lamella liquid crystals or (curved) monoolein-based cubic liquid crystalline phase. The authors found that the interaction mechanism for the NPs depended dramatically on the membrane topology.

There are several review articles on the study of model membranes, for recent examples the reader is encouraged to read Ref. [150].

1.3.4.2 Self assembly of polymer micelles

Three block polymers, consisting of polyethylene-oxide and polypropylene-oxide, may form micelles above a critical concentration solved in water. These micelles may self-assemble in different phases [165]. Similar to shear [166] an interface imposes anisotropy and texture may develop in the case when crys-

talline structures are formed [167]. The degree of texture depends on the affinity of the micelle corona to the coating of the substrate [8]. Further it was shown with NR that the addition of magnetic NP to the crystalline micellar solution may result in a micro shear effect, if a magnetic field is applied, which leads to the alignment of crystallites [168]. The depth dependence of the structure can be directly extracted from a single GISANS measurement by using the time of flight method, as the penetration depth of neutrons into the liquid depends on the wavelength for a given incident beam angle. It turns out that texture is most pronounced directly at the interface and decays with increasing distance from it, approaching a bulk powder structure [164]. Moreover, a clear difference in texture is seen depending on the surface energy of the substrate (see Fig. 1.9). By combining GISANS, NR and OSS, as shown in Fig. 1.4, a wide range of length scales can be investigated. This allows study of the formation of structure by measuring the texture and crystallite size. First, small crystallites form at an interface. These grow until they touch each other, which results in the alignment of their crystal axis and decrease of crystallite size [9]. Moreover, it turns out that a memory effect is present whether the crystalline phase is entered from low or high temperatures. During heating, micelles cubically dense pack at the interface, while during cooling hexagonal dense packing is reported [169]. For highly textured crystals it turns out that additional shear reduces the layering, which is different from bulk, where texture is introduced by the application of shear. After the cessation of shear the crystalline structure relaxes. This process is slower and less pronounced at interfaces where the micelles have the tendency to form well defined layers without shear and may stick [170].

1.3.4.3 Dynamics in bicontinuous polymer systems

The molecular dynamics of a bicontinuous microemulsion adjacent to a planar hydrophilic silicon surface was studied with GINSES. In a GINSES experiment, the evanescent wave with a scattering depth Λ probes the dynamical contrast of structures with a length Λ next to the substrate (typically a few 100 Å), while the scattering vector Q probes the structural length $l = \frac{2\pi}{Q}$ (typically a few 10 Å). Most experiments are conducted when the two length scales Λ and l are very different, and then the separation of length scales applies [171]. This means that the dynamics at length l is probed, while the depth Λ is highlighted.

At the surface, the microemulsion forms lamellar order [172]. Due to an increasing number of perforations with increasing depth, the microemulsion is slowly adapted to the bicontinuous sponge structure in the bulk (Fig. 1.10, inset). The selected scattering vector $Q = 0.08 \text{ \AA}^{-1}$ aims at independent membrane motions on length scales of $\approx 80 \text{ \AA}$. The measured relaxation time as a function of the scattering depth Λ displays a transition from the faster near surface relaxations to the slower bulk relaxations (see Fig. 1.10) [173]. The continuous red line was motivated by structural measurements of the lamellar order with increasing scattering depth. In this way, a continuous interpolation of relaxation times is

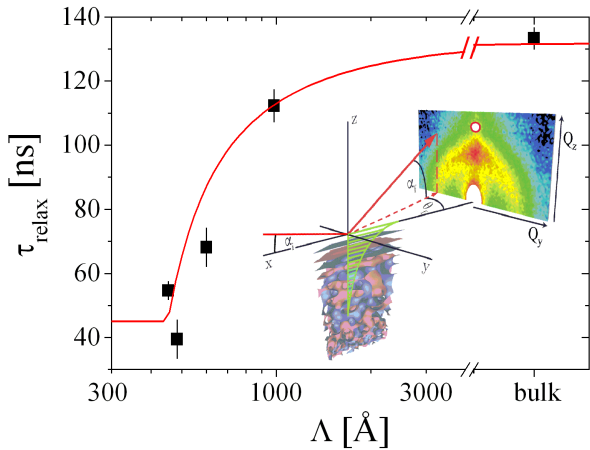


FIGURE 1.10 The relaxation times extracted from GINSES on a bicontinuous bulk microemulsion as a function of the scattering depth. By the evanescent wave (also indicated by the green shaded region) the near surface lamellar structure is highlighted to a different degree, according to the scattering depth. The NSE intensity is collected at $Q = 0.08 \text{ \AA}^{-1}$, i.e. beyond the correlation peak from the microemulsion, in order to focus on surfactant membrane fluctuations.

achieved. The faster near-surface motions are subject to the volume conservation of water or oil between the substrate and the first membrane or between the perfect lamellae. This scenario is also connected to the lubrication effect that describes a facilitated flow of lamellae along the planar substrate [174].

The near-surface dynamics of microemulsions was also studied for dispersed clay platelets [175]. Here, the maximum length scale of membrane fluctuations was given by the platelet diameter. This study then motivated the rheological study where clay platelets of different diameter were dispersed in either water or microemulsion [176]. In the flow field, the platelets are oriented along the flow direction. The aqueous dispersion displayed a strong growth of viscosities with increasing platelet diameter that reflects a stronger rigidity (and an additional criticality that cannot be discussed here). In a microemulsion, the trend is opposed due to the length scale cutoff of the membrane fluctuations (and more obviously the lubrication effect). The achieved high viscosities are interesting for food applications, while the low viscosities are interesting when fluids need to be pumped in tubes. The same publication [176] also addressed the flow of crude oils with dispersed clay, where strongly decreased viscosities were achieved at low temperatures. The lamellar arrangement of domains of the complex fluid "crude oil" is the explanation for that favorable behavior.

1.4 CONCLUSIONS AND OUTLOOK

NR is a powerful method for the study of solid-liquid boundaries. This is a consequence of the penetration power of neutrons for many engineering materials, as e.g. silicon, and the large scattering cross section of light elements. NR measurements provide direct access to the depth profile of isotopes as well as the magnetic induction across interfaces. Moreover, contrast variation experiments, utilising hydrogen/deuterium exchange, provide unique information about the conformation and concentration of components in liquids and polymers. As a consequence specular NR experiments became a standard and widely used method for the study of solid-liquid boundaries. OSS and GISANS provide unique information about correlations in the plane of an interface over length scales from nm to tens of μm . Energy resolved experiments even allow the investigation of fluctuations at the interface. However, these methods are less common, as neutron beams typically are not of very high brilliance. This scenario is currently changing as more and more dedicated instrumentation and new experimental approaches become available. Even more, with the European Spallation Source becoming available soon a significant improvement in performance of neutron instrumentation can be expected and grazing incidence scattering studies of solid-liquid boundaries may become even wider spread.

Acknowledgement

GAP and MWR acknowledge the Knut and Alice Wallenberg Foundation (Project No. KAW2012.0078) and the Swedish Foundation for Strategic Research ("REFIT" Project No. EM16-0013) for their financial support. MW acknowledges the Swedish research council for funding the national infrastructure Super ADAM. Becky Welbourn from INTER, Sarah Rogers from SANS2D, Andy Nelson from PLATYPUS and Alexei Vorobiev from Super ADAM beamlines are fulsomely thanked.

BIBLIOGRAPHY

- [1] L. Nevot, P. Croce, Characterization of surfaces by grazing x-ray reflection - application to study of polishing of some silicate-gasses, *Revue de Physique Appliquée* 15 (3) (1980) 761–779.
- [2] L. Parratt, Surface studies of solids by total reflection of x-rays, *Physical Review* 95 (2) (1954) 359–369.
- [3] O. S. Heavens, Optical properties of thin films, *Rep. Prog. Phys.* 23 (1960) 1.
- [4] C. F. Majkrzak, N. F. Berk, Exact determination of the phase in neutron reflectometry, *Phys. Rev. B* 52 (1995) 10827.
- [5] B. P. Toperberg, Polarized neutron reflectometry of magnetic nanostructures, *The Physics of Metals and Metallography* 116 (2015) 1337.
- [6] H. Zabel, K. Theis-Bröhl, M. Wolff, B. P. Toperberg, Polarized neutron reflectometry for the analysis of nanomagnetic systems, *IEEE Transactions on Magnetics* 44 (2015) 1928.
- [7] M. Wolff, A. Magerl, H. Zabel, Structure of polymer micelles close to the solid interface -

- a grazing incidence small angle neutron scattering study, *The European Physical Journal E* 16 (2) (2005) 141–145.
- [8] M. Wolff, U. Scholz, R. Hock, A. Magerl, V. Leiner, H. Zabel, Crystallization of micelles at chemically terminated interfaces, *Physical Review Letters* 92 (25).
- [9] M. Wolff, A. Magerl, H. Zabel, Crystallization of soft crystals, *Langmuir* 25 (1) (2009) 64–66. URL <http://pubs.acs.org/doi/abs/10.1021/la803015t>
- [10] A. Hafner, P. Gutfreund, B. P. Toperverg, A. O. F. Jones, J. P. de Silva, A. Wildes, H. E. Fischer, G. M., M. Sferrazza, Combined specular and off-specular reflectometry: elucidating the complex structure of soft buried interfaces, *J. Appl. Cryst.* 54 (2021) 924.
- [11] M. Wolff, Grazing incidence scattering, *EPJ Web of Conferences* 188 (2018) 04002.
- [12] M. Bee, Quasielastic neutron scattering, Adam Hilger, 1988.
- [13] R. Hempelmann, Quasielastic Neutron Scattering and Solid State Diffusion, Clarendon Press, 2000.
- [14] D. Richter, M. Monkenbusch, A. Arbe, J. Colmenero, Neutron spin echo in polymer systems, *Neutron Spin Echo in Polymer Systems* (2005) 1–221.
- [15] M. Monkenbusch, D. Richter, High resolution neutron spectroscopy—a tool for the investigation of dynamics of polymers and soft matter, *Comptes rendus physique* 8 (7-8) (2007) 845–864.
- [16] M. Wolff, A. Devishvili, J. A. Dura, F. A. Adlmann, B. Kitchen, G. K. Pálsson, H. Palonen, B. B. Maranville, C. F. Majkrzak, B. P. Toperverg, Nuclear spin incoherent neutron scattering from quantum well resonators, *Phys. Rev. Lett.* 123 (2019) 016101.
- [17] S. Jakusch, O. Holderer, M. Gvaramia, M. Ohl, M. Monkenbusch, H. Frielinghaus, Nanoscale rheology at solid-complex fluid interfaces, *Scientific Reports* 7 (2017) 4417.
- [18] A. R. Rennie, M. S. Hellsing, E. Lindholm, A. Olsson, Nanoscale rheology at solid-complex fluid interfaces, *Rev Sci Instrum* 86 (2015) 016115.
- [19] D. P. Hoogerheide, J. A. Dura, B. B. Maranville, C. F. Majkrzak, Low-background neutron reflectometry from solid/liquid interfaces, *Journal of Applied Crystallography* 55 (1) (2022) 58–66.
- [20] G. A. Pilkington, K. Harris, E. Bergendal, A. B. Reddy, G. K. Palsson, A. Vorobiev, O. N. Antzutkin, S. Glavatskikh, M. W. Rutland, Electro-responsivity of ionic liquid boundary layers in a polar solvent revealed by neutron reflectance, *Journal of Chemical Physics* 148 (2018) 193806.
- [21] J. N. Israelachvili, D. Tabor, The measurement of van der waals dispersion forces in the range 1.5 to 130 nm, *Proceedings of the Royal Society of London. A. Mathematical and Physical Sciences* 331 (1584) (1972) 19–38.
- [22] G. Binnig, C. F. Quate, C. Gerber, Atomic force microscope, *Physical review letters* 56 (9) (1986) 930.
- [23] Z. Mu, F. Zhou, S. Zhang, Y. Liang, W. Liu, Effect of the functional groups in ionic liquid molecules on the friction and wear behavior of aluminum alloy in lubricated aluminum-on-steel contact, *Tribology International* 353 (2005) 239.
- [24] T. Cosgrove, P. Luckham, R. Richardson, J. Webster, A. Zarbakhsh, The measurement of volume fraction profiles for adsorbed polymers under compression using neutron reflectometry, *Colloids and Surfaces A: Physicochemical and Engineering Aspects* 86 (1994) 103–110.
- [25] T. Cosgrove, J. S. Phipps, R. M. Richardson, M. L. Hair, D. A. Guzonas, Surface force and neutron scattering studies on adsorbed poly (2-vinylpyridine)-b-polystyrene, *Colloids and Surfaces A: Physicochemical and Engineering Aspects* 86 (1994) 91–101.
- [26] T. Cosgrove, A. Zarbakhsh, P. F. Luckham, M. L. Hair, J. R. Webster, Adsorption of polystyrene–poly (ethylene oxide) block copolymers on quartz using a parallel-plate surface-

- force apparatus and simultaneous neutron reflection, *Faraday Discussions* 98 (1994) 189–201.
- [27] J.-H. J. Cho, G. S. Smith, W. A. Hamilton, D. J. Mulder, T. L. Kuhl, J. Mays, Surface force confinement cell for neutron reflectometry studies of complex fluids under nanoconfinement, *Review of Scientific Instruments* 79 (10) (2008) 103908.
- [28] T. L. Kuhl, G. S. Smith, J. N. Israelachvili, J. Majewski, W. Hamilton, Neutron confinement cell for investigating complex fluids, *Review of Scientific Instruments* 72 (3) (2001) 1715–1720.
- [29] W. M. De Vos, L. L. Mears, R. M. Richardson, T. Cosgrove, R. M. Dalgiesh, S. W. Prescott, Measuring the structure of thin soft matter films under confinement: A surface-force type apparatus for neutron reflection, based on a flexible membrane approach, *Review of Scientific Instruments* 83 (11) (2012) 113903.
- [30] S. B. Abbott, W. M. de Vos, L. L. Mears, R. Barker, R. M. Richardson, S. W. Prescott, Hydration of odd–even terminated polyelectrolyte multilayers under mechanical confinement, *Macromolecules* 47 (10) (2014) 3263–3273.
- [31] W. M. De Vos, L. L. Mears, R. M. Richardson, T. Cosgrove, R. Barker, S. W. Prescott, Nonuniform hydration and odd–even effects in polyelectrolyte multilayers under a confining pressure, *Macromolecules* 46 (3) (2013) 1027–1034.
- [32] S. B. Abbott, W. M. de Vos, L. L. E. Mears, B. Cattoz, M. W. A. Skoda, R. Barker, R. M. Richardson, S. W. Prescott, Is osmotic pressure relevant in the mechanical confinement of a polymer brush?, *Macromolecules* 48 (7) (2015) 2224–2234.
- [33] S. B. Abbott, W. M. de Vos, L. L. Mears, M. Skoda, R. Dalgiesh, S. Edmondson, R. M. Richardson, S. W. Prescott, Switching the interpenetration of confined asymmetric polymer brushes, *Macromolecules* 49 (11) (2016) 4349–4357.
- [34] I. J. Gresham, B. A. Humphreys, J. D. Willott, E. C. Johnson, T. J. Murdoch, G. B. Webber, E. J. Wanless, A. R. Nelson, S. W. Prescott, Geometrical confinement modulates the thermoresponse of a poly (n-isopropylacrylamide) brush, *Macromolecules* 54 (5) (2021) 2541–2550.
- [35] J. F. Gonzalez-Martinez, H. Boyd, P. Gutfreund, R. J. Welbourn, C. Robertsson, C. Wickström, T. Arnebrant, R. M. Richardson, S. W. Prescott, R. Barker, et al., Muc5b mucin films under mechanical confinement: a combined neutron reflectometry and atomic force microscopy study, *Journal of Colloid and Interface Science*.
- [36] M. Wolff, P. Kuhns, G. Liesche, J. F. Ankner, J. F. Browning, P. Gutfreund, Combined neutron reflectometry and rheology, *Journal of Applied Crystallography* 46 (6) (2013) 1729–1733.
- [37] F. A. Adlmann, P. Gutfreund, J. F. Ankner, J. F. Browning, A. Parizzi, B. Vacaliuc, C. E. Halbert, J. P. Rich, A. J. C. Dennison, M. Wolff, Towards neutron scattering experiments with sub-millisecond time resolution, *J. Appl. Cryst.* 48 (2015) 220.
- [38] P. Ball, Water as an active constituent in cell biology, *Chemical Reviews* 108 (1) (2008) 74–108, pMID: 18095715.
- [39] T. Thorsen, S. Maerkli, S. Quake, Microfluidic large-scale integration, *Science* 298 (5593) (2002) 580–584.
- [40] M. Maccarini, Water at solid surfaces: A review of selected theoretical aspects and experiments on the subject, *Biointerphases* 2 (3) (2007) MR1–MR15.
- [41] R. Steitz, T. Gutberlet, T. Hauss, B. Klösgen, R. Krastev, S. Schemmel, A. C. Simonsen, G. H. Findenegg, Nanobubbles and their precursor layer at the interface of water against a hydrophobic substrate, *Langmuir* 19 (6) (2003) 2409–2418.
- [42] Y.-S. Seo, S. Satija, No intrinsic depletion layer on a polystyrene thin film at a water interface, *Langmuir* 22 (17) (2006) 7113–7116.
- [43] X. H. Zhang, A. Khan, W. A. Ducker, A nanoscale gas state, *Physical Review Letters* 98

- (2007) 136101.
- [44] A. Carambassis, L. C. Jonker, P. Attard, M. W. Rutland, Forces measured between hydrophobic surfaces due to a submicroscopic bridging bubble, *Physical Review Letters* 80 (1998) 5357.
 - [45] N. Ishida, T. Inoue, M. Miyahara, K. Higashitani, Nano bubbles on a hydrophobic surface in water observed by tapping-mode atomic force microscopy, *Langmuir* 16 (2000) 6377.
 - [46] J. W. G. Tyrrell, P. Attard, Images of nanobubbles on hydrophobic surfaces and their interactions, *Physical Review Letters* 87 (17) (2001) 176104.
 - [47] D. A. Doshi, E. B. Watkins, J. N. Israelachvili, J. Majewski, Reduced water density at hydrophobic surfaces: Effect of dissolved gases, *Proceedings of the National Academy of Sciences of the United States of America* 102 (27) (2005) 9458–9462.
 - [48] M. Mezger, H. Reichert, S. Schröder, J. Okasinski, H. Schröder, H. Dosch, D. Palms, J. Ralston, V. Honkimäki, High-resolution *in situ* x-ray study of the hydrophobic gap at the water-octadecyl-trichlorosilane interface, *Proceedings of the National Academy of Sciences of the United States of America* 103 (49) (2006) 18401–18404.
 - [49] X. H. Zhang, A. Quinn, W. A. Ducker, Nanobubbles at the interface between water and a hydrophobic solid, *Langmuir* 24 (9) (2008) 4756–4764, pMID: 18366225.
 - [50] S. Karpitschka, E. Dietrich, J. R. T. Seddon, H. J. W. Zandvliet, D. Lohse, H. Riegler, Nonintrusive optical visualization of surface nanobubbles, *Physical Review Letters* 109 (2012) 066102.
 - [51] H. Peng, G. R. Birkett, A. V. Nguyen, Progress on the surface nanobubble story: What is in the bubble? why does it exist?, *Advances in Colloid and Interface Science* 222 (0) (2015) 573.
URL <http://www.sciencedirect.com/science/article/pii/S0001868614002516>
 - [52] P. Ball, Nanobubbles are not a superficial matter, *ChemPhysChem* 13 (8) (2012) 2173–2177.
 - [53] P. Gutfreund, M. Maccarini, A. C. J. Dennison, M. Wolff, The search for nanobubbles by using specular and off-specular neutron reflectometry, *Langmuir* 32 (2016) 9091.
 - [54] O. I. Vinogradova, Drainage of a thin liquid film confined between hydrophobic surfaces, *Langmuir* 11 (1995) 2213.
 - [55] M. Wolff, B. Akgun, M. Walz, A. Magerl, H. Zabel, Slip and depletion in a newtonian liquid, *Europhysics Letters* 82 (3) (2008) 1–5.
 - [56] P. Gutfreund, M. Wolff, M. Maccarini, S. Gerth, J. F. Ankner, J. F. Browning, C. E. Halbert, H. Wacklin, H. Zabel, Depletion at solid/liquid interfaces: Flowing hexadecane on functionalized surfaces, *The Journal of Chemical Physics* 134 (2011) 064711.
 - [57] E. Lauga, M. P. Brenner, H. A. Stone, Microfluidics: The no-slip boundary condition, in: C. Tropea, A. L. Yarin, J. F. Foss (Eds.), *Springer Handbook of Experimental Fluid Mechanics*, Springer, 2007, pp. 1219–1240.
 - [58] H.-G. Steinrück, A. Magerl, M. Deutsch, B. M. Ocko, Pseudorotational epitaxy of self-assembled octadecyltrichlorosilane monolayers on sapphire (0001), *Physical Review Letters* 113 (2014) 156101.
 - [59] P. Gutfreund, O. Bäumchen, R. Fetzer, D. van der Grinten, M. Maccarini, K. Jacobs, H. Zabel, M. Wolff, Solid surface structure affects liquid order at the polystyrene–self-assembled-monolayer interface, *Physical Review E* 87 (2013) 012306.
 - [60] W. A. Ducker, T. J. Senden, R. M. Pashley, Direct measurement of colloidal forces using an atomic force microscope, *Nature* 38 (1991) 725.
 - [61] M. J. Earle, K. R. Seddon, Ionic liquids. green solvents for the future, *Pure and Applied Chemistry* 72 (2000) 1391.
 - [62] S. Glavatskikh, E. Hoglund, Tribtronics : towards active tribology, *Tribology International*

- 41 (2008) 934.
- [63] H. A. Spikes, Triboelectrochemistry: Influence of applied electrical potentials on friction and wear of lubricated contacts, *Tribology Letters* 68 (2020) 90.
- [64] J. Sweeney, F. Hausen, R. Hayes, G. B. Webber, F. Endres, M. W. Rutland, R. Bennewitz, R. Atkin, Control of nanoscale friction on gold in an ionic liquid by a potential-dependent ionic lubricant layer, *Physical Review Letters* 109 (2012) 155502.
- [65] M. Z. Bazant, B. D. Storey, A. A. Kornyshev, Double layer in ionic liquids: Overscreening versus crowding, *Phys. Rev. Lett.* 106 (2011) 046102.
- [66] S. Watanabe, G. A. Pilkington, A. Oleshkevych, P. Pedraz, M. Radiom, R. Welbourn, S. Glavatskikh, M. W. Rutland, Interfacial structuring of non-halogenated imidazolium ionic liquids at charged surfaces: effect of alkyl chain length, *Physical Chemistry Chemical Physics* 22 (2020) 8450.
- [67] P. K. Cooper, H. Li, N. R. Yepuri, A. Nelson, G. B. Webber, A. P. Le Brun, T. A. Darwish, G. G. Warr, R. Atkin, Ionic liquid adsorption at the silica–oil interface revealed by neutron reflectometry, *The Journal of Physical Chemistry C* 122 (2018) 14077.
- [68] F. U. Shah, S. Glavatskikh, D. R. MacFarlane, A. Somers, M. Forsyth, O. N. Antzutkin, Novel halogen-free chelated orthoborate–phosphonium ionic liquids: synthesis and tribophysical properties, *Physical Chemistry Chemical Physics* 13 (2011) 12865.
- [69] G. A. Pilkington, A. Oleshkevych, P. Pedraz, S. Watanabe, M. Radiom, A. B. Reddy, A. Vorobiev, S. Glavatskikh, M. W. Rutland, Electroresponsive structuring and friction of a non-halogenated ionic liquid in a polar solvent: effect of concentration, *Physical Chemistry Chemical Physics* 22 (2020) 19162.
- [70] D. Wakeham, P. Niga, G. G. Warr, M. W. Rutland, R. Atkin, Nonionic surfactant adsorption at the ethylammonium nitrate surface: A neutron reflectivity and vibrational sum frequency spectroscopy study, *Langmuir* 26 (2010) 8313.
- [71] O. Y. Fajardo, F. Bresme, A. A. Kornyshev, M. Urbakh, Water in ionic liquid lubricants: Friend and foe, *ACS Nano* 11 (2017) 6825.
- [72] P. F. Choong, M. M. Dowswy, The grand challenge - managing end-staged joint osteoarthritis, *Front. Surg.* 1 (2014) 9.
- [73] B. A. Hills, Surface-active phospholipid: a pandora's box of clinical applications. part ii. barrier and lubricating properties, *International Medicine Journal* 32 (2002) 242.
- [74] B. A. Hills, Molecular mechanisms of synovial joint lubrication, *Proceedings of the Institution of Mechanical Engineers, Part J: Journal of Engineering Tribology* 220 (2006) 691.
- [75] J. Seror, L. Zhu, R. Goldberg, A. J. Day, J. Klein, J. supramolecular synergy in the boundary lubrication of synovial joints, *Net. Commun.* 6 (2015) 6497.
- [76] M. K. Kosinska, G. Liebisch, G. Lochnit, J. Wilhelm, H. Klein, U. Kaesser, G. Lasczkowski, M. Rickert, G. Schmitz, J. Steinmeyer, A lipidomic study of phospholipid classes and species in human synovial fluid, *Arthritis & Rheumatism* 65 (9) (2013) 2323–2333.
- [77] T. Kawano, H. Miura, T. Mawatari, T. Moro-Oka, Y. Nakanishi, H. Higaki, Y. Iwamoto, Mechanical effects of the intraarticular administration of high molecular weight hyaluronic acid plus phospholipid on synovial joint lubrication and prevention of articular cartilage degeneration in experimental osteoarthritis, *Arthritis & Rheumatism* 48 (7) (2003) 1923–1929.
- [78] L. L. E. Mears, S. B. Abbott, R. D. Barker, W. M. de Vos, S. W. Prescott, R. M. Richardson, Structural evidence for a reinforcing response and retention of hydration during confinement of cartilage lipids, *Frontiers in Physics* 9.
- [79] M. Kreuzer, M. Strobl, M. Reinhardt, M. C. Hemmera, T. Hauß, R. Dahint, R. Steitz, Impact of a model synovial fluid on supported lipid membranes, *Biophys. Acta* 1818 (2012) 2648.

- [80] F. Schwörer, M. Trapp, X. Xu, O. Soltwedel, J. Dzubiella, R. Steitz, R. Dahint, Drastic swelling of lipid oligobilayers by polyelectrolytes: A potential molecular model for the internal structure of lubricating films in mammalian joints, *Langmuir* 34 (4) (2018) 1287–1299.
- [81] F. Schwörer, M. Trapp, M. Ballauff, R. Dahint, R. Steitz, Surface-active lipid linings under shear load—a combined in-situ neutron reflectivity and atr-ftir study, *Langmuir* 31 (42) (2015) 11539–11548.
- [82] M. Kreuzer, M. Trapp, R. Dahint, R. Steitz, Polymer-induced swelling of solid-supported lipid membranes, *Membranes* 6 (1).
- [83] G. W. Greene, R. Thapa, S. A. Holt, X. Wang, C. J. Garvey, R. F. Tabor, Structure and property changes in self-assembled lubricin layers induced by calcium ion interactions, *Langmuir* 33 (10) (2017) 2559–2570.
- [84] J. F. Gonzalez-Martinez, H. Boyd, P. Gutfreund, R. J. Welbourn, C. Robertsson, C. Wickström, T. Arnebrant, R. M. Richardson, S. W. Prescott, R. Barker, J. Sotres, Muc5b mucin films under mechanical confinement: A combined neutron reflectometry and atomic force microscopy study, *Journal of Colloid and Interface Science* 614 (2022) 120–129.
- [85] I. Berts, G. Fragneto, J. Hilborn, A. R. Rennie, Tuning the density profile of surface-grafted hyaluronan and the effect of counter-ions, *Euro. Phys. J. E Soft Matter* 36 (2013) 70.
- [86] A. Dedinaite, P. M. Claesson, Synergies in lubrication, *Phys. Chem. Chem. Phys.* 19 (2017) 23677.
- [87] O. Azzaroni, Polymer brushes here, there, and everywhere: Recent advances in their practical applications and emerging opportunities in multiple research fields, *Journal of Polymer Science Part A: Polymer Chemistry* 50 (16) (2012) 3225–3258.
- [88] J. B. Field, C. Toprakcioglu, R. C. Ball, H. B. Stanley, L. Dai, W. Barford, J. Penfold, G. Smith, W. Hamilton, Determination of end-adsorbed polymer density profiles by neutron reflectometry, *Macromolecules* 25 (1) (1992) 434–439.
- [89] D. Perahia, D. G. Wiesler, S. K. Satija, L. J. Fetters, S. K. Sinha, S. T. Milner, Neutron reflectivity of end-grafted polymers: Concentration and solvent quality dependence in equilibrium conditions, *Physical Review Letters* 72 (1994) 100–103.
- [90] A. Karim, S. K. Satija, J. F. Douglas, J. F. Ankner, L. J. Fetters, Neutron reflectivity study of the density profile of a model end-grafted polymer brush: Influence of solvent quality, *Physical Review Letters* 73 (1994) 3407–3410.
- [91] C. Devaux, F. Cousin, E. Beyou, J.-P. Chapel, Low swelling capacity of highly stretched polystyrene brushes, *Macromolecules* 38 (10) (2005) 4296–4300.
- [92] J. R. Ell, D. E. Mulder, R. Faller, T. E. Patten, T. L. Kuhl, Structural determination of high density, atrp grown polystyrene brushes by neutron reflectivity, *Macromolecules* 42 (24) (2009) 9523–9527.
- [93] I. Hiotelis, A. G. Koutsoubas, N. Spiliopoulos, D. L. Anastassopoulos, A. A. Vradis, C. Toprakcioglu, A. Menelle, G. Sakellariou, N. Hadjichristidis, Neutron reflectivity and computer simulation studies of self-assembled brushes formed by centrally adsorbed star polymers, *Macromolecules* 41 (20) (2008) 7648–7655.
- [94] N. Spiliopoulos, A. G. Koutsoubas, D. L. Anastassopoulos, A. A. Vradis, C. Toprakcioglu, A. Menelle, G. Mounrichas, S. Pispas, Neutron reflectivity study of free-end distribution in polymer brushes, *Macromolecules* 42 (16) (2009) 6209–6214.
- [95] L. Léger, E. Raphal, H. Hervet, Surface-anchored polymer chains: Their role in adhesion and friction, in: *Polymers in confined environments*, Vol. 138 of *Adv. Polymer Sci.*, Springer, 1999, pp. 185–225.
- [96] C. Marzolin, P. Auroy, M. Deruelle, J. P. Folkers, L. Léger, A. Menelle, Neutron reflectometry

- study of the segment-density profiles in end-grafted and irreversibly adsorbed layers of polymer in good solvents, *Macromolecules* 34 (25) (2001) 8694–8700.
- [97] H. Yim, M. S. Kent, S. Mendez, S. S. Balamurugan, S. Balamurugan, G. P. Lopez, S. Satija, Temperature-dependent conformational change of pnipam grafted chains at high surface density in water, *Macromolecules* 37 (5) (2004) 1994–1997.
 - [98] H. Yim, M. S. Kent, S. Satija, S. Mendez, S. S. Balamurugan, S. Balamurugan, G. P. Lopez, Evidence for vertical phase separation in densely grafted, high-molecular-weight poly(*n*-isopropylacrylamide) brushes in water, *Phys. Rev. E* 72 (2005) 051801.
 - [99] T. J. Murdoch, B. A. Humphreys, J. D. Willott, K. P. Gregory, S. W. Prescott, A. Nelson, E. J. Wanless, G. B. Webber, Specific anion effects on the internal structure of a poly(*n*-isopropylacrylamide) brush, *Macromolecules* 49 (16) (2016) 6050–6060.
 - [100] I. J. Gresham, T. J. Murdoch, E. C. Johnson, H. Robertson, G. B. Webber, E. J. Wanless, S. W. Prescott, A. R. J. Nelson, Quantifying the robustness of the neutron reflectometry technique for structural characterization of polymer brushes, *Journal of Applied Crystallography* 54 (3) (2021) 739–750.
 - [101] S. Christau, T. Möller, F. Brose, J. Genzer, O. Soltwedel, R. von Klitzing, Effect of gold nanoparticle hydrophobicity on thermally induced color change of PNIPAM brush/gold nanoparticle hybrids, *Polymer (Guildf.)* 98 (2016) 454–463.
 - [102] D. Nguyen, C. J. Clarke, A. Eisenberg, M. H. Rafailovich, J. Sokolov, G. S. Smith, Investigation of polymer brushes and adsorbed layers under shear, *Journal of Applied Crystallography* 30 (5 Part 2) (1997) 680–683.
 - [103] S. M. Baker, G. S. Smith, D. L. Anastassopoulos, C. Toprakcioglu, A. A. Vradis, D. G. Bucknall, Structure of polymer brushes under shear flow in a good solvent, *Macromolecules* 33 (4) (2000) 1120–1122.
 - [104] R. Ivkov, P. D. Butler, S. K. Satija, L. J. Fetters, Effect of solvent flow on a polymer brush: A neutron reflectivity study of the brush height and chain density profile, *Langmuir* 17 (10) (2001) 2999–3005.
 - [105] D. L. Anastassopoulos, N. Spiliopoulos, A. A. Vradis, C. Toprakcioglu, S. M. Baker, A. Menelle, Shear-induced desorption in polymer brushes, *Macromolecules* 39 (26) (2006) 8901–8904.
 - [106] D. L. Anastassopoulos, N. Spiliopoulos, A. A. Vradis, C. Toprakcioglu, A. Menelle, F. Cousin, Neutron reflectivity study of end-adsorbed bimodal polymer systems under static conditions and shear flow, *Macromolecules* 46 (17) (2013) 6972–6980.
 - [107] A. Korolkovas, P. Gutfreund, A. Chennevière, J. F. Ankner, F. A. Adlmann, M. Wolff, J.-L. Barrat, Shear deformation of low-density polymer brushes in a good solvent, *Phys. Rev. E* 98 (2018) 032501.
 - [108] A. Korolkovas, C. Rodriguez-Emmenegger, A. de los Santos Pereira, A. Chennevière, F. Restagno, M. Wolff, F. A. Adlmann, A. J. C. Dennison, P. Gutfreund, Polymer brush collapse under shear flow, *Macromolecules* 50 (3) (2017) 1215–1224.
 - [109] T. Koga, Y. Ji, Y. S. Seo, C. Gordon, F. Qu, M. H. Rafailovich, J. C. Sokolov, S. K. Satija, Neutron reflectivity study of glassy polymer brushes in density fluctuating supercritical carbon dioxide, *Journal of Polymer Science Part B: Polymer Physics* 42 (17) (2004) 3282–3289.
 - [110] M. Reinhardt, J. Dzubiella, M. Trapp, P. Gutfreund, M. Kreuzer, A. H. Gröschel, A. H. E. Müller, M. Ballauff, R. Steitz, Fine-tuning the structure of stimuli-responsive polymer films by hydrostatic pressure and temperature, *Macromolecules* 46 (16) (2013) 6541–6547.
 - [111] I. Rodriguez-Loureiro, E. Scoppola, L. Bertinetti, A. Barbutta, G. Fragneto, E. Schneck, Neutron reflectometry yields distance-dependent structures of nanometric polymer brushes interacting across water, *Soft Matter* 13 (34) (2017) 5767–5777.

- [112] S. Micciulla, Y. Gerelli, R. A. Campbell, E. Schneck, A versatile method for the distance-dependent structural characterization of interacting soft interfaces by neutron reflectometry, *Langmuir* 34 (3) (2018) 789–800.
- [113] G. Decher, Fuzzy nanoassemblies: Toward layered polymeric multicomposites, *Science* 277 (5330) (1997) 1232–1237.
- [114] J. Schmitt, T. Gruenewald, G. Decher, P. S. Pershan, K. Kjaer, M. Lüsche, Internal structure of layer-by-layer adsorbed polyelectrolyte films: a neutron and x-ray reflectivity study, *Macromolecules* 26 (25) (1993) 7058–7063.
- [115] R. Steitz, V. Leiner, R. Siebrecht, R. v. Klitzing, Influence of the ionic strength on the structure of polyelectrolyte films at the solid/liquid interface, *Colloids Surf. A Physicochem. Eng. Asp.* 163 (1) (2000) 63–70.
- [116] R. Koehler, R. Steitz, R. von Klitzing, About different types of water in swollen polyelectrolyte multilayers, *Adv. Colloid Interface Sci.* 207 (2014) 325–331.
- [117] M. Lüsche, J. Schmitt, G. Decher, W. G. Bouwman, K. Kjaer, Detailed structure of molecularly thin polyelectrolyte multilayer films on solid substrates as revealed by neutron reflectometry, *Macromolecules* 31 (25) (1998) 8893–8906.
- [118] A. Sill, P. Nestler, A. Weltmeyer, M. Paßvogel, S. Neuber, C. A. Helm, Polyelectrolyte multilayer films from mixtures of polyanions: Different compositions in films and deposition solutions, *Macromolecules* 53 (16) (2020) 7107–7118.
- [119] Y. E. Ghoussoub, M. Zerball, H. M. Fares, J. F. Ankner, R. von Klitzing, J. B. Schlenoff, Ion distribution in dry polyelectrolyte multilayers: a neutron reflectometry study, *Soft Matter* 14 (9) (2018) 1699–1708.
- [120] S. Dodox, R. Steitz, A. Laschewsky, R. von Klitzing, Effect of ionic strength and type of ions on the structure of water swollen polyelectrolyte multilayers, *Phys. Chem. Chem. Phys.* 13 (21) (2011) 10318–10325.
- [121] O. Ivanova, O. Soltwedel, M. Gopinadhan, R. Köhler, R. Steitz, C. A. Helm, Immobile light water and Proton-Deuterium exchange in polyelectrolyte multilayers, *Macromolecules* 41 (19) (2008) 7179–7185.
- [122] M. Zerball, A. Laschewsky, R. Köhler, R. Von Klitzing, The effect of temperature treatment on the structure of polyelectrolyte multilayers, *Polymers (Basel)* 8 (4) (2016) 120.
- [123] H. W. Jomaa, J. B. Schlenoff, Salt-induced polyelectrolyte interdiffusion in multilayered films: A neutron reflectivity study, *Macromolecules* 38 (20) (2005) 8473–8480.
- [124] O. Soltwedel, P. Nestler, H.-G. Neumann, M. Paßvogel, R. Köhler, C. A. Helm, Influence of polycation (PDADMAC) weight on vertical diffusion within polyelectrolyte multilayers during film formation and postpreparation treatment, *Macromolecules* 45 (19) (2012) 7995–8004.
- [125] P. Nestler, M. Paßvogel, H. Ahrens, O. Soltwedel, R. Köhler, C. A. Helm, Branched poly(ethylenimine) as barrier layer for polyelectrolyte diffusion in multilayer films, *Macromolecules* 48 (23) (2015) 8546–8556.
- [126] M. Paßvogel, P. Nestler, R. Köhler, O. Soltwedel, C. A. Helm, Influence of binary polymer mixtures on the nonlinear growth regimes of polyelectrolyte multilayer films, *Macromolecules* 49 (3) (2016) 935–949.
- [127] A. Sill, P. Nestler, A. Azinfar, C. A. Helm, Tailorable polyanion diffusion coefficient in LbL films: The role of polycation molecular weight and polymer conformation, *Macromolecules* 52 (22) (2019) 9045–9052.
- [128] V. Selin, J. F. Ankner, S. A. Sukhishvili, Diffusional response of layer-by-layer assembled polyelectrolyte chains to salt annealing, *Macromolecules* 48 (12) (2015) 3983–3990.
- [129] S. Micciulla, O. Soltwedel, O. Lömann, R. von Klitzing, Temperature responsive behavior of

- polymer brush/polyelectrolyte multilayer composites, *Soft Matter* 12 (4) (2016) 1176–1183.
- [130] O. Löhmann, S. Micciulla, O. Soltwedel, E. Schneck, R. von Klitzing, Swelling behavior of composite systems: Mutual effects between polyelectrolyte brushes and multilayers, *Macromolecules* 51 (8) (2018) 2996–3005.
- [131] D. Boyaciyan, L. Braun, O. Löhmann, L. Silvi, E. Schneck, R. von Klitzing, Gold nanoparticle distribution in polyelectrolyte brushes loaded at different ph conditions, *J. Chem. Phys.* 149 (16) (2018) 163322.
- [132] T. Kyrey, M. Ganeva, K. Gawlitza, J. Witte, R. von Klitzing, O. Soltwedel, Z. Di, S. Wellert, O. Holderer, Grazing incidence SANS and reflectometry combined with simulation of adsorbed microgel particles, *Physica B Condens. Matter* 551 (2018) 172–178.
- [133] T. Kyrey, J. Witte, V. Pipich, A. Feoktystov, A. Koutsoubas, E. Vezhlev, H. Frielinghaus, R. von Klitzing, S. Wellert, O. Holderer, Influence of the cross-linker content on adsorbed functionalised microgel coatings, *Polymer (Guildf.)* 169 (2019) 29–35.
- [134] J. Witte, T. Kyrey, J. Lutzki, A. M. Dahl, M. Kühnhammer, R. v. Klitzing, O. Holderer, S. Wellert, Looking inside poly(n-isopropylacrylamide) microgels: Nanomechanics and dynamics at solid–liquid interfaces, *ACS Appl. Polym. Mater* 3 (2) (2021) 976–985.
- [135] K. Gawlitza, O. Ivanova, A. Radulescu, O. Holderer, R. von Klitzing, S. Wellert, Bulk phase and surface dynamics of PEG microgel particles, *Macromolecules* 48 (16) (2015) 5807–5815.
- [136] S. Wellert, Y. Hertle, M. Richter, M. Medebach, D. Magerl, W. Wang, B. Demé, A. Radulescu, P. Müller-Buschbaum, T. Hellweg, R. von Klitzing, Inner structure of adsorbed ionic microgel particles, *Langmuir* 30 (24) (2014) 7168–7176.
- [137] R. E. Rosenzweig, *Ferrohydrodynamics*, Cambridge University Press, 1985.
- [138] E. Blums, A. Cebers, M. M. Maiorov, *Magnetic Fluids*, W. de Gruyter, 1997.
- [139] R. Schmidt, J. Benkoski, K. Caviccia, A. Karim, *Soft Matter* 7 (2011) 5756.
- [140] M. Grzelczak, J. Vermant, E. M. Furst, L. M. Liz-Marzán, Directed self-assembly of nanoparticles, *ACS Nano* 4 (2010) 3591.
- [141] G. M. Whiteside, B. Grzybowski, Self-assembly at all scales, *Science* 295 (2002) 2418.
- [142] G. A. Ozin, K. Hou, B. V. Lotsch, B. L. Cademartiri, D. P. Puzzo, F. Scatognella, A. Ghadimi, J. Thomson, Nanofabrication by selfassembly, *Mater. Today* 12 (2009) 12.
- [143] J. Faraudo, J. S. Andreu, C. Calero, J. Camacho, Predicting the self-assembly of superparamagnetic colloids under magnetic fields, *Adv. Funct. Mater.* 26 (2016) 3837.
- [144] A. Vorobiev, J. Major, H. Dosch, G. Gordeev, D. Orlova, Magnetic field dependent ordering in ferrofluids at sio2 interfaces, *Phys. Rev. Lett.* 93 (2004) 267203.
- [145] A. Saini, K. Theis-Bröhl, A. Koutsoubas, K. L. Krycka, J. A. Borchers, M. Wolff, Magnetic particle self-assembly at functionalized interfaces, *Langmuir* 37 (2021) 4064.
- [146] A. Saini, J. A. Borchers, S. George, B. B. Maranville, K. L. Krycka, J. A. Dura, K. Theis-Bröhl, M. Wolff, Layering of magnetic nanoparticles at amorphous magnetic templates with perpendicular anisotropy, *Soft Matter* 16 (2020) 7676.
- [147] K. Theis-Bröhl, P. Gutfreund, A. Vorobiev, B. P. Wolff, M. Toperverg, J. A. Dura, J. A. Borchers, Magnetic particle self-assembly at functionalized interfaces, *Langmuir* 37 (2021) 4064.
- [148] T.-B. K., V. E. C., A. Gomez, H. D. L., A. Saini, M. Wolff, B. B. Maranville, E. Brok, K. K. L., J. Dura, B. J. A., Self-assembled layering of magnetic nanoparticles in a ferrofluid on silicon surfaces, *ACS Appl. Mater. Interfaces* 10 (2018) 5050.
- [149] K. Theis-Bröhl, M. Saini, A. Wolff, J. A. Dura, B. B. Maranville, J. A. Borchers, Magnetic particle self-assembly at functionalized interfaces, *Langmuir* 37 (2021) 4064.
- [150] L. A. Clifton, R. A. Campbell, F. Sebastiani, J. Campos-Terán, J. F. Gonzalez-Martinez, S. Björklund, J. Sotres, M. Cárdenas, Design and use of model membranes to study biomolec-

- ular interactions using complementary surface-sensitive techniques, *Advances in Colloid and Interface Science* 277 (2020) 102118.
- [151] A. Åkesson, T. Lind, N. Ehrlich, D. Stamou, H. Wacklin, M. Cárdenas, Composition and structure of mixed phospholipid supported bilayers formed by popc and dppc, *Soft Matter* 8 (2012) 5658–5665.
 - [152] S. Waldie, T. K. Lind, K. Browning, M. Moulin, M. Haertlein, V. T. Forsyth, A. Luchini, G. A. Strohmeier, H. Pichler, S. Maric, M. Cárdenas, Localization of cholesterol within supported lipid bilayers made of a natural extract of tailor-deuterated phosphatidylcholine, *Langmuir* 34 (1) (2018) 472–479.
 - [153] A. Luchini, A. N. O. Nzulumike, T. K. Lind, T. Nylander, R. Barker, L. Arleth, K. Mortensen, M. Cárdenas, Towards biomimics of cell membranes: Structural effect of phosphatidylinositol triphosphate (pip3) on a lipid bilayer, *Colloids and Surfaces B: Biointerfaces* 173 (2019) 202–209.
 - [154] L. Caselli, A. Ridolfi, G. Mangiapia, P. Maltoni, J.-F. Moulin, D. Berti, N.-J. Steinke, E. Gustafsson, T. Nylander, C. Montis, Interaction of nanoparticles with lipid films: the role of symmetry and shape anisotropy, *Phys. Chem. Chem. Phys.* 24 (2022) 2762–2776.
 - [155] K. Browning, T. K. Lind, S. Maric, S. Malekkhiait-Häffner, G. Nordin-Fredrickson, E. Bengtsson, M. Malmsten, M. Cardenas, Asymmetric distribution of anionic phospholipids in supported lipid bilayers, *Sci. Reports* 7 (2017) 7478–7490.
 - [156] Y. Gerelli, L. Porcar, L. Lombardi, G. Fragneto, Lipid exchange and flip-flop in solid supported bilayers, *Langmuir* 29 (41) (2013) 12762–12769.
 - [157] S. Stanglmaier, S. Hertrich, K. Fritz, J.-F. Moulin, M. Haese-Seiller, J. O. Rädler, B. Nickel, Asymmetric distribution of anionic phospholipids in supported lipid bilayers, *Langmuir* 28 (29) (2012) 10818–10821.
 - [158] Y. Correa, S. Waldie, M. Thépaut, S. Micciulla, M. Moulin, F. Fieschi, H. Pichler, V. Trevor Forsyth, M. Haertlein, M. Cárdenas, Sars-cov-2 spike protein removes lipids from model membranes and interferes with the capacity of high density lipoprotein to exchange lipids, *Journal of Colloid and Interface Science* 602 (2021) 732–739.
 - [159] G. Pabst, J. Katsaras, V. A. Raghunathan, Enhancement of steric repulsion with temperature in oriented lipid multilayers, *Phys. Rev. Lett.* 88 (2002) 128101.
 - [160] S. Jaksch, F. Lipfert, A. Koutsoubas, S. Mattauch, O. Holderer, O. Ivanova, H. Frielinghaus, S. Hertrich, S. F. Fischer, B. Nickel, Influence of ibuprofen on phospholipid membranes, *Phys. Rev. E* 91 (2015) 022716.
 - [161] S. Jaksch, A. Koutsoubas, S. Mattauch, O. Holderer, H. Frielinghaus, Long-range excitations in phospholipid membranes, *Chemistry and Physics of Lipids* 225 (2019) 104788.
 - [162] S. Jaksch, A. Koutsoubas, S. Mattauch, O. Holderer, H. Frielinghaus, Measurements of dynamic contributions to coherent neutron scattering, *Colloids and Interfaces* 2 (3).
 - [163] S. Jaksch, O. Holderer, H. Frielinghaus, A. Koutsoubas, P. Zolnierczuk, D. W. Hayward, S. Förster, P. Müller-Buschbaum, Influence of nacl on the structure and dynamics of phospholipid layers, *Frontiers in Physics* 9.
 - [164] M. Wolff, J. Herbel, F. Adlmann, A. J. C. Dennison, G. Liesche, P. Gutfreund, S. Rogers, Depth-resolved grazing-incidence time-of-flight neutron scattering from a solid–liquid interface, *Journal of Applied Crystallography* 47 (1) (2014) 130–135.
 - [165] G. Wanka, H. Hoffmann, W. Ulbricht, Phase-diagrams and aggregation behavior of poly(oxyethylene)-poly(oxypropylene)-poly(oxyethylene) triblock copolymers in aqueous-solutions, *Macromolecules* 27 (15) (1994) 4145–4159.
 - [166] K. Mortensen, Structural studies of aqueous solutions of peo - ppo - peo triblock copolymers, their micellar aggregates and mesophases; a small-angle neutron scattering study, *Journal of*

- Physics: Condensed Matter 8 (1996) A103.
- [167] M. Wolff, A. Magerl, H. Zabel, Ns-sans for the investigation of micellar systems, Thin solid films 515 (2007) 5724.
 - [168] A. Saini, M. Wolff, Macroscopic alignment of micellar crystals with magnetic micro-shearing, Langmuir 35 (2019) 3980.
 - [169] N. Wolff, S. Gerth, P. Gutfreund, M. Wolff, Temperature dependent cubic and hexagonal packing in micellar structures, Soft Matter 10 (2014) 8420.
 - [170] M. Wolff, R. Steitz, P. Gutfreund, N. Voss, S. Gerth, M. Walz, A. Magerl, H. Zabel, Shear induced relaxation of polymer micelles at the solid-liquid interface, Langmuir 24 (20) (2008) 11331–11333.
 - [171] F. Lipfert, M. Kerscher, S. Mattauch, H. Frielinghaus, Stability of near-surface ordering of bicontinuous microemulsions in external shear-fields, Journal of colloid and interface science 534 (2019) 31–36.
 - [172] M. Kerscher, P. Busch, S. Mattauch, H. Frielinghaus, D. Richter, M. Belushkin, G. Gompper, Near-surface structure of a bicontinuous microemulsion with a transition region, Physical Review E 83 (3) (2011) 030401.
 - [173] H. Frielinghaus, M. Kerscher, O. Holderer, M. Monkenbusch, D. Richter, Acceleration of membrane dynamics adjacent to a wall, Physical Review E 85 (4) (2012) 041408.
 - [174] N. Gov, A. Zilman, S. Safran, Hydrodynamics of confined membranes, Physical Review E 70 (1) (2004) 011104.
 - [175] F. Lipfert, O. Holderer, H. Frielinghaus, M.-S. Appavou, C. Do, M. Ohl, D. Richter, Long wavelength undulations dominate dynamics in large surfactant membrane patches, Nanoscale 7 (6) (2015) 2578–2586.
 - [176] M. Gvaramia, G. Mangiapia, V. Pipich, M.-S. Appavou, S. Jaksch, O. Holderer, M. D. Rukhadze, H. Frielinghaus, Tunable viscosity modification with diluted particles: when particles decrease the viscosity of complex fluids, Colloid and Polymer Science 297 (11) (2019) 1507–1517.